Reply to comments on acp-2017-472

L. Schoon and Ch. Zülicke

March 23, 2018

1. Reply to Co-Editor

We appreciate the comments and recommendations of the Co-Editor to the revised manuscript and answer the risen up issues point-by-point. With Appendix A we provide details of our revised validation excersise. The revised manuscript with the highlighted changes can be found in Appendix B.

1) Reviewer 1 appreciates the addition of a methodology section to the manuscript. However, he/she has identified flaws and actually provides both IDL-code as well as result-plots achieved with this code to check your results. In your revised manuscript you will need to make sure that the methodology section is corrected.
We are very grateful for the hints of Reviewer 1 to ambiguities according the method comparison section. We revised it carefully (see Appendix A). Details can be found in the point-by-point-answer to the comments of Reviewer 1. Most relevant change was the use of a narrower box width which improved the results of the sinusoidal fit. However, the Hilbert transform performed best without any a-priori assumption. The provision of source code from the FZ Jülich helped considerably with this issue.

2) Reviewer 2 still insists that the manuscript should rather be split in two parts, one addressing the new methodology and one addressing the application of the methodology to obtain new scientific results. I understand that it is your approach to introduce the method and that you try to convince the reader of its usefulness by showing some initial, to some extent preliminary, results. This needs to be made clear from the text and also from the title.

I therefore request that you change the title of this manuscript to reflect this. A potential title could be: A novel method for the extraction of gravity wave parameters from gridded 3d data: method description and initial scientific results.
We agree with the Co-Editor that the focus of this publication is on the introduction of the new method and the scientific results are used to convince the reader on its usefulness. Thus, we kept the atmospheric dynamic discussion part short. We changed the title as suggested and added explicit formulation on this into the text.

3) Ideally, in order to improve the scientific quality of the second part of the manuscript, the analysis should be extended to time dependent data. If this proves to be beyond the scope of the present study I request that you state this explicitly and explain what steps will need to be taken.
We had a look at the temporal extend of the analysed mSSW and decided that this will be far beyond the scope of this paper. Indeed, we found several interesting transient features in this time. Their reasonable presentation, however, would require the presentation of wind and wave fields including indicators for their sources. Because this would add too much information to the present paper including the introduction of a new source diagnostics, we decided to leave this issue for a forthcoming paper. For now, we stay with the snapshots of horizontal and vertical sections of wave packets and focus on their interpretation, improve the quality of figures and add some more parameters to the interpretation. We are sure that our initial scientific discussion provided here shows the reader the unique usefulness of the method.

4) Besides the points that I have emphasized above, it goes without saying that also all other specific comments from both reviewers will need to be addressed as usual.
Detailed responses to each of the reviewers can be found below, including additional information in the Appendix.

2. Reply to Reviewer 1

The revised version of the paper is much improved. There is now a good motivation, the method description is stringent and the examples shown for the application are well chosen. However, in the method comparison S3D is not correctly applied. That is detailed in the major comment below and results for a correct application shown in the attached Figure. In addition, there are some inaccuracies in the description of the other methods.

You should also point out the basic assumption of attributing all variance to a single wave together with the method overview. Some additional specific comments are given below. If the method intercomparison will be corrected and the other comments taken into account I recommend publication of the manuscript in ACP.
Major comment:
You are using an 1D data set. At this you cannot apply S3D or 3DST. There are two ways attacking the problem:
a) You can expand the data set to a 3D data set.
b) You can use an 1D sinusoidal fit in a sliding window
These two possibilities are discussed here for S3D, code for reproduction is attached and can be run with the general IDL package of the Juelich remote sensing group.

a) In order to produce a data set comparable to normal S3D application, expansion of the test function to 3D should include a wave structure in the two other spatial dimensions as well. We can choose two ways of doing this:
a.1) Use the same wavelength for both wave packets
a.2) Use different wavelengths for bot wave packets
Employing a cube-volume of the size of 0.5 in the direction of the variation, a.1 (red) is very close to the solution of the Hilbert transform, a.2 (blue) can separate between the wavelengths and has a step-wise transition in wavenumber without the spurious wavenumbers between the two solutions. The results are shown in the attached figure, panels a (amplitude) and b (wavenumber). However, for real-world problems we probably would apply a size of 1.0 or 1.5 in order to get more confidence on not ideally-shaped wave patterns. In the case of box-size 1.5 (panels c and d) we find a notable smearing of the envelope (15% underestimation of the peak-amplitude), still closer to the reference than the Stockwell transform. All these fits draw information from the two additional directions which we have chosen to be homogeneous in amplitude and wavelength.
b) A mere 1D sinusoidal fit of window length 1.5 produces somewhat smeared amplitudes and some spurious oscillations (panels e and f). That can also be emulated by S3D and prescribing no wavelength information in the two additional directions (A.3).

For the paper you could follow one of the following two approaches:
1. Use the 1D solution. Do not call it S3D. Mention that the additional dimensions will add to the quality of the results
2. Discuss a.1/a.2 for a realistic window length of 1.5. Note in the text that the window

length has an influence.
We follow 1. And stay with one dimension according to the definition of the test case. In our view, the quality improvement from adding more dimensions is due to a certain phase average effect. With regard to the window width we use a size of 1.5 for the sinusoidal fit and found an acceptable amplitude. A further decrease of window width leads to a quality decrease for the wave number estimate. Numerous tests are documented in a technical report which we attach to the attention of the reviewer (Appendix A). In the text of the paper, we extend the documentation on the setup for the alternative diagnosis methods including statements on the influence of the window size.

Anyway, none of this approaches performs as lousy as the so-called S3D solution in the method intercomparison.
In the paper, we used a window of 7.85 for all the box-based methods (sinusoidal fit and auto-correlation function analysis). This was oriented on a-priori reasoning that the largest wavelength should be at least five times covered by the window. We had in mind the statistical significance of the wave number estimate, and not the best-possible spatial resolution. However, in order to be practical, we performed a number of tests and finally adopted those a-priori windows which lead to the best results in both amplitude and wave number. See attached technical report (Appendix A).

Similarly, the Stockwell transform could perform better than in this test. There is a tuning factor c to reduce the width of the Gaussian envelope and also for the ST the third dimension adds information. One could thus also tune ST for a closer match in the 3D case. Also this should shine up in the discussion
We hesitate to tune the Stockwell transform because the advantageous variance conservation would be violated (see Appendix A). This reasoning is now included in the text.

Summarizing: the idea of a simple method intercomparison adds value to the paper, but it must be done right!
The width of the box window is the major responsible for the quality of the box-based methods. Now, we have decreased the window width which improved the quality, and we have completed the documentation of the method intercomparison.

Minor comments:
P4L7 The importance of oblique propagation is not restricted to the mesosphere. Ehard

et al show this for the mid stratosphere but it may be quite substantial already in the UTLS (e.g. Krisch et al). Oblique propagation hence just redistributes selective transmission and makes the analysis more complicated. It is definitely a limiting factor for the interpretation of vertical profiles and some discussion should be added.
We add the fact that oblique propagation plays an important role from UTLS to the mesosphere and point out clearer that we focus on vertical propagation.

P3L4 In principle you should be able to calculate time-space spectra of u and w and calculate cospectra for the respective wave modes (e.g. Alexander et al. 2004). This is not limited by the size of the analysis volume and can be used to apply zonal mean quantities. Given that one reviewer asked for the motivation to use horizontal divergence, that is still not sufficiently motivated. One motivation could be the correction terms which need to be applied for the influence of Coriolis force on pseudomomentum flux.
The main motivation of using the horizontal divergence is that we get ageostrophic wave components without the necessity of filtering data beforehand. This is given on P2. In the analysis part of the paper we derive the wave action from the horizontal divergence and choose this quantity to be the centre of our discussion.
Generally, with the help of dispersion relations several quantities can be estimated with the results of UWaDi, like the zonal vertical pseudo momentum flux, etc. We waive these possibilities to not blow up this paper.

Figure 5c and interpretation: The vertical wavelength is shortest in the wind maximum and then increases(!) towards where you assume the critical level is. There is only a very small peak at that altitude (much longer wavelengths than at the assumed excitation altitudes), comparable in size to other local variations. There are a number of explanations beside critical level which could explain your finding of a maximum in the jet, for instance oblique propagation, partial reflection ... So, if you want to retain this discussion, you should offer more proof and infer the phase speed for the considered waves considering the phase shift between two consecutive time steps of ECMWF.
We added Figure 6 to perform this discussion more in detail. We show the intrinsic frequency, horizontal wavelength and horizontal phase speed. We find the critical level by a rotation of the wave vector and showing that the horizontal phase speed equals the background wind speed.

Specific comments:

P1L25 S3D without hyphen
We changed the notation from S-3D to S3D.

P2L1 Ern and Preusse, 2012 and Ern et al. 2014 use different methods -> omit
We omitted those.

P2L2 to P2L18 What you say is all correct, but I think you are missing the chance to set this in a broader context. The fundamental problem of all wave analyses methods is given by the fact that you have to compromise between spatial and spectral resolution (cf. the uncertainty relation). A second point is to which extent the sampling and total volume will influence the result. Going along such lines you can order along the spatial resolution:
Fourier Transform: Assumes homogeneity of amplitudes and phases through hole considered volume. Wavelengths determined by volume size. Covers whole spectrum continously. No information loss.
3DST: Assumes homogeneity inside a volume corresponding to one wavelength (or fraction, cf. scaling factor). Wavelengths limited by size of total analysis volume. Selecting largest events implies loss of variance (information).
*S3D: Assumes homogeneity inside an predefined analysis volume. Restriction to wavelength by cube size (sensitivity study: reliable for wavelength < 2.5*cube size). Outcome depends on pre-selected cube size. Selecting leading (not largest) components implies loss of variance (information).*
Clearer argumentation considering the suggestions of Reviewer 1 on S3D and 3D ST was added.

Hilbert Transform: Does not assume homogeneity. No limitation on wavelengths except Nyquist. Gives information of amplitude and phase, wavelength information inferred from local phase gradient -> all variance is attributed to one wave mode. This prize you have to pay is important and should be mentioned for a fair assessment!
We edited this part considering this suggestions.

Anyway, if you present these different compromises between wave resolution and spatial resolution you can claim that Hilbert transform provides the one we are missing. UWADI thus provides the user with a complementary tool for investigating wave events.
All localized methods can be shifted by steps smaller than the analysis method, so one

is, in principle, able to calculate wave parameters for each original point for 3DST and S3D. A large asset of the Hilbert transform is that it is computationally cheap.
Some more discussion on that was added to the validation of the method section 2.2.

More specific:
P2L2 "two" is most often chosen, but not a general limitation. However, as you say in your next sentence, always a small number is taken. I would just omit the "two".
We just omitted the "two".

P2L8 3DST, please use notations as in the reference papers
In Lehmann et al. (2012) the notation "S3D" is used. We adopted that. In Wright et al. (2017) the notations "3-D ST" and "S3-D" occur. To compromise we use for the Stockwell method "3D ST" now.

P2L11 The only assumption made is that of upward propagating waves. This ambiguity between e.g. eastward-upward and westward-downward cannot be decided from temperature observations alone and is not a restriction of the method.
We omitted this mistakable statement.

P2L12 S3D uses the largest described variance, i.e. minimum chi-square to pick the wave, 3DST the largest amplitudes. In both cases it can be more than one wave. Anyway, that should not be relevant for what you want to say, perhaps: Both S3D and 3DST use a small number of the most-prominent waves. This leaves some variance unattributed and hence means a loss of information.
We follow the suggestion and added that statement.

What perhaps is more important in this context: Both methods implicitly assume homogeneity of amplitude and wave vector, S3D inside one analysis volume, 3DST inside a volume corresponding to one wavelength. This is a loss of spatial information.
As mentioned before, we edited the method introduction part as well as the comparison section and are sure that the pros and cons of the different methods are clearer now.

P2L27 to make clear it is not flow over convection: by flow over orography, by convection ...
The "by" is added.

P4L18 use e.g. for the reference
The "e.g." is added.

P4L22 The phase of the wave ...
Edited.

P6L4 Alienation of outliers is taken care of by two different quality. Please reformulate
The word "checks" was missing.

P8L11 You can focus on these scales. However, a vertical limit of 15km will lead to shift part of the spectrum in and out the so-chosen visibility filter (Alexander, JGR, 1998 and later literature on this topic).
The authors added some discussion on observational filter limitations and provide for one of the vertical profiles additionally horizontal wavelength, horizontal phase speed and intrinsic frequency to make sure to not misinterpret the wave behaviour due to e.g. refraction of the wave outside of our filter limits.

*P8L27 do not interact with the mean flow. *W*ave action*
In order to avoid confusion we reformulated this passage.

P9L8 In order to make the paper easier to read you could indicate by the notation whether a quantity is intrinsic or ground based; e.g. use $\hat{\omega}$ and c_g.
The notation was changed.

P9L9 The wind also needs to be constant in time. Perhaps better turn around: If the wind ... Quote a ray-tracing paper, e.g. Lighthill or Marks and Eckermann.
Our discussion is based on a stationary homogeneous background wind which only varies in vertical direction. This is now stated in the text. Any deeper discussions on wave propagation in a time-depented mean flow will be part of an upcoming paper. We make this clearer in some reformulations throughout the revised manuscript.

P9L14 swap the two sentences: The displaced ... The jet streak ...
Swapped.

P9L16 I am wondering: is eastern Siberia really a comparable situation to Europe? The GW fronts seem more aligned than across the winds and there is less deceleration but strong curvature.
The formulation was misleading. We reformulated that parts considering your comment.

P9L23 However, it is counter-intuitive. Both a stronger damping and a coarser vertical grid would let expect the shorter waves to be more strongly damped. Did you try what happens if you increase the upper limit of your analysis range?
After the first round of revision we concentrated on finding the right data and focussed on comparing different data resolutions with the same setting of our method. This is discussed in Sec.2.3. In so far, the indicated decreasing wavelength above 50 km did not depend on the horizontal resolution. It appeared for different wind conditions (compare the zonal mean profile and case ③). Finally, we could not find a proofable explanation of this behaviour. In order to concentrate the paper on the methodology, we eliminated all kinds of interpretations of the topic of sponge layer and damping to not run into too much speculation. This is not a topic that can be discussed satisfactorily as we follow the editor's advice to concentrate on the method.

*Fig 2: Omit ** on the exponents.*
Omitted

Fig 3: Please generate a second panel with zonal mean wind and N. At constant c_g, k vertical wavelength is inversely proportional to N, so you should see that as well.
A second panel is created which completes the diagnosed wave numbers with the apparent (ground-based) phase speed and allows for the evaluation of passive upward propagation. We did not plot N because it is a parameter in the estimation of intrinsic frequency and phase speed. The latter would enter a relation like $\lambda_z = \frac{2\pi}{N}\hat{c}$ and insofar we could not isolate the impact of N. Such an investigation would require the diagnosis of the ground-based (apparent) frequency or phase in seldom situations with changing N over constant u.

Fig 4: It is evident, still: Give the units of the shown quantities, please.
The units are added.

P9L30 ? height range ?

Meant was longitudinal. Changed.

P10L1 descented -> descended ?
Yes, changed.

It would be nice to indicate the profile locations in Fig 2a.
We agree and added the circled profile numbers to this figure.

P10L7/L9 2 Overall*
Reformulated.

P10L10 ... remains constant. Puzzling, that's in the sponge.
The wave action remains constant above 25 km altitude. The first sponge starts at 30 km. We reformulated this sentence, but the main statement remains true.

P12L7 This could be one of the major assets of a local method - that one sees the scaling of the wave properties with the varying wind ...
Yes, and we show this asset with the other local profiles. In profile ① the scaling is restricted by the smoothing inside our method. We find it important to mention this restriction.

P12L13 At these altitudes, GWs of vertical wavelength ...
We added your suggestions.

P12L19 an SSW (i.e. an EsEsDoubleU)
The whole text was searched and all "n"s added.

P12L21 They point out theoretically that during the upward propagation of GWs these waves (comma, upward)
Comma and "s" are deleted.

P12L22 Actually that was profile-based MEM/HA (Preusse et al, JGR, 2002) with a 10km running window. For current day limb sounders we get only an estimate of the absolute horizontal wavelength and do not estimate wave action.
We omitted this statement.

P12L25 the longest vertical wave length with 7 km If that were really the longest existing wavelengths AIRS should not see any GWs at all. There should be also cases of substantially longer wavelengths.
We do not state that this is the longest possible wavelength for GWs. We find this wavelength with the limits of our vertical bandpass filter of 1 km to 15 km because we are interested in GWs emitted from jets that are supposed to have wavelengths in this limit. Nevertheless, we reformulated that statement to make clearer that it is the longest wavelengths according to our method settings.

P12L26 Scandinavian
Changed to capital "S".

P14L12 put -> exerted
Changed, the whole paragraph was reformulated.

P14L17 jet-generated GWs tend to have such phase speeds. (convection would be much faster).
Changed, the whole paragraph was reformulated.

P14L19 relatively high
Changed, the whole paragraph was reformulated.

P14L27 Low wind speed and low wave action, maybe. In cases of larger waves these may still dominate the statistical effects leading to the higher wavenumbers.
We deleted the discussion part on the sponge layer according to Reviewer 2 to avoid an incidentally discussion of a topic that could fill another whole paper.

P14L32 such -> thus ? or omit it
Omitted.

P15L2 nomination -> assumption or attribution of the variance to
Changed accordingly.

3. Reply to Reviewer 2

Review
Diagnosis of Local Gravity Wave Properties during a Sudden Stratospheric Warming
by
Lena Schoon and Christoph Zülicke
The paper's intention is to diagnose local properties of gravity waves (essentially, amplitude and wavenumber vector) from 3D gridded data by a tool named "UWaDi". The paper essentially consists of two portions. One part is the presentation of the wave diagnosis tool and the second part describes an application to 3D IFS analyses for one selected day in January 2016. Unfortunately, both parts are half-baked. And both parts would gain immensely if they were written such as they were individual scientific contributions to this journal. Part 1: The presentation of a new software tool (line 13, page 1: "Here, we want to introduce a new method named "Unified Wave Diagnosis" (UWaDi).") which is coded with open source software should be happily resolved by offering it also as open source code. Currently, the standard is to publish the open source software under a certain license and to allow access to the code via a repository. Requests to the authors (line 24, page 15) are simply not up-to-date as authors might leave institutions, for example. There are other remarks concerning the outline and scope of the "UWaDi"-tool which are listed below.
With regard to the publication of source code and any used data we follow the guidelines of the journal. Next to that, we will provide the manual of the method as well as a list of publications containing results obtained by UWaDi on a web page of the authors institute, the Leibniz-Institute of Atmospheric Physics Kühlungsborn. The source code of the method will be provided upon request until this first method-introducing publications is still not finally published regularly to make sure that if the source code is used by others, correct citation is possible.

Part 2: At some places in the text, the authors try to state their scientific goals which shall be tackled with the "UWaDI"-tool: line 1, page 1 ("The selective transmission of gravity waves through an inhomogeneous mean flow is investigated.", line 7, page 3: "We are interested in the longitude-dependent transmission of GWs during a SSW."). This is a relevant topic; however, the results presented shed only some spotlight on the whole dynamical processes during the selected period. Only one selected time is considered and both the temporal process of propagating waves (transmission) and the specification of

the wave sources remain rather speculative. As above: the paper would greatly benefit if this part is separated from the paper and investigated in an own, full-length scientific contribution.

We follow the suggestions of the editor and reformulated the title as well as some specific statements in the text concerning our scientific goals for this paper. We point out more clearly that the focus on the paper lies on the introduction of the method. The scientific discussion is kept short, restrictions are named and further analyses containing temporal evolution and source discussion are mentioned to be subject of future studies. The application case here is used to show the reader that the method can be used to find local spatial wave packets in a dynamically inhomogeneous situation. See also the reply to the editor (Sec. 1).

Specific Remarks

Abstract:

- it should be mentioned right at the beginning that the method is only applicable for gridded 3D data

Now it is mentioned in the title, by suggestion of the editor.

- line 3: "wave properties": they should be listed here for completeness

They are listed now.

- line 3: "wave-containing data" should be specified; later, this turns out to be a crucial point of the analysis where a preselection of wave modes is made by the choice of the horizontal divergence as "wave containing data"; furthermore, the retrieval of this field in a specified spectral resolution certainly impacts the results which is not discussed in the paper at all

The separation of wave and background from each other is not topic of this paper. The method needs a wave signal at the beginning. By choosing the horizontal divergence we count for the dynamical filtering of the geostrophic and ageostrophic flow. In the ongoing paper we derive the wave action from the horizontal divergence as the discussed quantity.

The method includes a bandpass filter. The method attributes all variance to one wave mode, therefore this filter indicates the finding of the waves the user is interested in.

Information on the resolution of the used data is added.

- line 7: scientific result: "confirm locally different transmission"; rather weak statement: as no propagation is investigated but only still images are presented you can only refer to "appearance" of gravity waves under the given background conditions (see your own statement in line 14, page 3)
As mentioned above, we keep the scientific discussion short to keep the introduction of the new method in the focus of the paper. We changed this statement to "appearance" according your suggestion.

- line 8: I thought, the local wavenumbers are the output of the tool; why "additionally ..."?
This is a misunderstanding. The method gives the amplitude and the three-dimensional wave number. Thus, the wave number is an additional output. Nevertheless, we omit it.

- line 9: very speculative statement
If this refers to the hint on a GW generated by the stratospheric jet, we give more hints on that in the discussion part of the paper now. It is also noted further scientific investigation is intended. This is adequately addressed in the abstract. This issue will be studied in a forthcoming paper.

Introduction:
- it is certainly an advantage to discuss and compare the different methods for the retrieval of wave properties; there are two points which should be added. First: make clear that "UWaDi" needs regularly gridded data from the very first beginning to point out the difference to other methods. Second, I miss the state-of-the-art review of the application of Hilbert transforms to atmospheric data in 3D. For example, the sentences in the paragraph about the Hilbert transform (page 2, 3rd para) can lead to a misunderstanding: "Kinoshita and Sato (2013) provide a three-dimensional application on Rossby and GWs. Our method comes up with an enhancement for three dimensions and the additionally provision of the wave number in every dimension which was not presented before." as they give the impression that K&S2013 use the Hilbert transform. Unfortunately, the word "Hilbert transform" does not appear in that paper. Maybe, I didn't read the paper carefully enough but I suggest to check this statement and to add appropriate applications of Hilbert transforms in atmospheric 3D data discussing their advantages and disadvantages (Glatt and Wirth, you know these papers).

Referring to your point 1: The title and abstract were changed according to that.
Referring to your point 2: We apologize and corrected the citation. It has to be Sato et al. (2013). Glatt and Wirth (2014) do not use the Hilbert transform in three dimensions. They operate on a longitude-plane and perform the Hilbert Transform for every latitude seperately. We added that.

- the scientific focus on the characterization of gravity waves appearing in high-resolution IFS data is good; the authors have all means at hand to provide a substantial contribution; however, this would be a full paper and not only an addition to the presentation of "UWaDI". See part 2 above!
Indeed, this kind of paper is in preparation which builds on the first scientific results which are given in this publication.

- line 16, page 3: the full set of output of "UWaDi" is unclear to me: Is "...we will use "UWaDi" with a GW-specific diagnostic." an addition or the standard set?
We further extended the method-description part to make that clearer. This specific statement is omitted now, to not rise up unclarities at this point of the paper. What was meant is that UWaDi can be used to obtain waves of any kind of wavelengths. By choosing the limits of the implemented bandpass filter one restricts the results to a specific wave set. We are interested in GWs, therefore we adapt the UWaDi algorithm to that.

- the intention to study a period which is " ... very well sampled with observations of GW properties" (line 29, page 3) is very good; unfortunately, the authors do not use them; furthermore, they use a quantity to identify waves which is hardly measurable ("Our approach concentrates on fields of horizontal divergence of ECMWF IFS data", line 2, page 4); for atmospheric physicists, temperature fluctuations would be a much better choice!
Throughout the paper we mention several times that we chose a period of time where measurement campaigns took place. Therefore, these period is very well sampled with observations. We further mention, that it is our aim to contribute to the results of these measurement campaigns with our findings.
The second point of using the horizontal divergence was already discussed above. We choose the horizontal divergence to avoid the separation of wave and background. We use the horizontal divergence to derive the wave action as the analysed quantity. We mention that UWaDi can be used with any other input quantity which contains a wave

signal. If someone wants to use wind or temperature fluctuations this is truly possible. (No 3)

- line 32/33, page 3: I would recommend to avoid such strong statements as "Even the T799 resolution gives proof of correct GW appearance in the stratosphere."
As recommended, we avoid such statements.

lines 5 -9, page 4: As mentioned above, I have problems to see a discussion about propagation (vertical or horizontal) when you only provide one time snapshots. This must be speculative.
We reformulated this part to make clear what our purpose is. "We concentrate on vertical profiles of GW appearance to give a first impression of the functionality of the this method."

Method and Data
(a) The description of the first step (page 4 and 5) is totally incomprehensible: "Horizontally, the grids are equidistant if they are provided on a regular latitude-longitude grid." I don't think, this statement can be true if distance is measured in meters. Please, provide the correct formulas how you compute the distances for the regular lat-lon grid. This should be specified in a step-by-step outline of the method!
We added more information on that in the description part. Point 1 describes the calculation of grid points.

"Vertical interpolation from model levels to equidistant height levels is performed by associating constant heights with pressure levels."
I don't understand this. First of all: are you using IFS data on pressure or model levels? How do you determine the height on these levels? And how do you interpolate the data on an equidistant altitude grid?
Point No 2 in the step-by-step outline answers these questions now.

"Consider to first separate the fluctuations from the background with appropriate numerical or dynamical filters." I have no idea what the sentence means and what you are referring to.
Point No 3 of the step-by-step outline was reformulated.

(b) You outline the method for 1D fields. Could you specify what f_x means?! Is this f(x,y_f,z_f,t_f) ?? Subscripts "_f" mean at fixed positions or time?
We added a sentence to explain the indices in Point No 4.

(c) Is Eq (10) correct? delta denotes horizontal divergence, right?! Shouldn't be the "delta" in the formulae a "sigma" as f_x is the divergence in your applications, correct??
Yes, you are correct. The sigma was added, as well as a symbol description. No 11.

(d) Figure 1: Why do you plot negative amplitudes when Eq. (11) takes the positive square-root? What are the thin black lines? The choice of colors could be changed to improve readability.
The negative amplitude is shown to include positive and negative variations of the wave packet amplitude. A description on the thin lines (the envelope) is added.
Colours were changed.

(e) The subsection about the IFS data must be improved. Please, provide the following information and avoid discussions about other cycles here:
- IFS cycle 41r1 is used; (if you really want to refer to differences of 41r1 to other cycles, see Ehard et al, 2018: Comparing ECMWF high resolution analyses to lidar temperature measurements in the middle atmosphere. Q.J.R. Meteorol. Soc. doi:10.1002/qj.3206;)
The discussion part on the other cycles is omitted and the reference included.

For which spectral resolution you retrieve the data from the archive?
T511. Information added on P9L??

Maybe, I have to mention that the retrieval of data goes along in a two-step procedure. You can retrieve data using the full set of spectral coefficients (in MARS retrieval RESOL=AV) or you can specify a zonal wavenumber (e.g., RESOL=309) you want. If you do not specify anything, default values are chosen, see: https://software.ecmwf.int/wiki). After this first step, the data are interpolated on a given grid (specification of the GRID parameter in the retrieval).
- on which regular lat/lon grid are the data interpolated to?
As mentioned in the text the grid size we find adequate is 0.36.

- do you use data on pressure or model levels?
Already answered. Model levels.

- how do you compute the altitude on these levels?
Already answered.

(f) Section 2.4 and Appendix B Equation (14) cannot be derived by the relations provided in appendix B.
*Appendix B: The Appendix is about the "Derivation of the TOTAL wave energy" not only about the kinetic one. The presented equations cannot lead to the final result (B4). There is a mistake (I think, omega is missing) in the provided formula for vorticity tendency (line 23, page 16). Actually, zeta is the default symbol for relative vorticity not xi. Referring to two text books (Vallis, Eq 4.69, Gill, Eq. 7.10.7), the formula for the absolute vorticity in a rotating frame of reference is D(zeta+f)/Dt = - (f+zeta)*delta. Why do you obviously use d zeta/dt=-f*delta only? Discuss this approximation! Furthermore, I obtain different signs in (B3) when I use the provided relations between vorticity and divergence and between divergence and vertical velocity. Please, check!!*
We are grateful to the reviewer to have inspected the mathematical section. The typos have been eliminated, we use ζ for the vertical vorticity component and specify the kind of approximation used. Actually, these are the primitive equations in f plane Boussinesq approximation linearised around a resting environment as appropriate for hydrostatic inertia-gravity waves (see Gill, section 8.4., for example).

line 8, page 9: What is Omega?
Description added.

Results
- for which time the analysis is performed?
0UTC. Added to the text.

- line 14, page 9: Change formulation "The jet streak above northern Europe is decelerating" if you just refer to the wind inside the jet. If you refer to the propagation of the jet streak itself and its deceleration, you should provide evidence.
The statement is reformulated.

- line 16: "Equal patterns appear above eastern Siberia .." I cannot see EQUAL patterns.
The statement is reformulated.

- Fig 2b is not mentioned in the text, but reference to it fits in line 16.
Reference added.

- The details in Figure 2 are hardly visible. Maybe, different line increments might increase the readability.
Line thicknesses, color scales and line increments are changed. Fig2

- line 20: If it is "more convenient in terms of wavelengths" you should plot them instead of wavenumbers in the respective Figures 3 and 5
All plots show wavelengths now. Fig3, Fig5, Fig6.

- line 21: I found an upper limit at 196 km (2 pi/3.2 10-5 m-1) not 165 km.
With the new plots this paragraph was rewritten.

- line 20 and line 21: the horizontal wavenumber changes by about 66%, the vertical only by about 45% over the height region. Thus, the statement: "In the zonal mean the horizontal wave number remains nearly constant with increasing altitude" cannot be supported by the data provided in Fig. 3.
The part was reformulated including additional information on the horizontal phase speed.

- very speculative and not provided by evidence: "independent from the overall synoptic situation and is therefore expected to be an artefact of artificial wave damping from the IFS sponge layer." (line 24, page 9)
To avoid any misinterpretations we omit the discussion on damping.

- I do not get the meaning of "We did not find significant differences between spatial averaging over areas of some longitudes extension and the local profiles (not shown)." What mean areas? Do you also average zonally?
This was added in the course of revision process 1 because one reviewer had doubts that local profiles show reliable results compared to zonal averaged profiles. We did several case studies and found that the local profiles show as good results as the regional avera-

ged ones. As our purpose is to show the advantages of local wave analysis we mention here, what we have found. Nevertheless, to not cause any misunderstandings, we again omit this statement.

- line 29, page 9: "The low-pass filter applied in Step 8 helps to overcome massive grid-point to grid-point fluctuations." The documentation of this step could be a nice addition to a more substantial documentation of Part 1 (above).
In the course of deleting the sentence before, this statement was omitted as well. See above.

- line 1, page 10: do you really mean "descented"?
Typo. Corrected to descended.

- line 9, page 10: "The not trustworthy areas are excluded." See above for Part 1.
It is mentioned in no 2 that areas of high orography provide misleading results. We refer to that here. The statement was reformulated.

- line 12, page 12: "Altogether, GW emissions seems to take place in the .." and line 16, same page "..Mountains, hence, mountain waves are most likely." are very speculative and not fully supported by the data provided. This issue would belong to the Part 2 of the a possible separated paper.
The statement was reformulated to GW activity.

Discussion
first paragraph: "These findings were obtained with the box-based S-3D algorithm. We add some spatially more refined analysis with UWaDi." What about to really apply the other methods used for the comparision with the synthetic data to the real case considered here? This would add substance!
A proven statement on the quality of a method can be made only if the results are known beforehand. Therefore, we choose the Zimin test case. Otherwise you can not decide which number is nearer to “truth” than others.

line 27, page 12: " ... and agree with findings of Limpasuvan et al. (2011)." and line 29: " ... This is close to the findings of Krisch et al. (2017), who .." If you really intent a quantitative comparision, I would recommend to avoid statements like those. The

Limpasuvan case lacks comparability in the background wind field, I guess. And, it is not clear what exactly you compare and refer to. The Krisch case is even more dangerous as they point at the dominant horizontal propagation which is omitted here.
According to your suggestion we omit the comparison to Krisch et al. (2017). The comparison to Limpasuvan et al. (2011) was reformulated. They did show that during an SSW westward propagating GWs emanate from key topographic features around the polar edge. They also find that these GWs have long vertical wavelengths. This fits to our findings and is worth to be mentioned in the discussion.

line 30, page 12: there is no evidence of data to provide a proof of the statement " ... from the 25 January to 30 January the overall approaching flow direction did not change above northern Europe and comparable GW characteristics can be expected."
Statement omitted.

line 4, page 14: again, the hypothesis of a wave source at the stratospheric jet remains hypothetical unless more facts of evidence are provided. The geographical association of large wave action with the nose of the jet does not mean undoubtedly that the jet is the source.
See answer below, as this topics belong together.

line 15..., page 14: the identification of a critical level by detecting a local maximum in k_z is a possible choice which alone is not sufficient to proof the critical level absorption. As you have all tools at hand, why you do not derive the group and phase velocities of wave packets and identify their sources? This would give much stronger evidence.
We adopted the suggestion to include more diagnosed wave characteristics for a more detailed documentation. We decided to do so for the zonal mean profiles and case 2. In these profiles there are no critical (Jones) levels present, and thats why we did not mention them any more. Instead we used the additional data for argumentation against passive propagation and for jet-related sources.

line 19/20, page 14: I don't understand "The near-inertial GWs are not subject of absorption." Why?? There exists so-called Jones critical levels.
This discussion was revised. See above.

Summary and Conclusions

I would have expected here NEW insights into the scientific topics which were mentioned in the Introduction and in the Abstract: "The selective transmission of gravity waves through an inhomogeneous mean flow is investigated." One finds a summary of "UWaDI" and potential future developments "UWaDi may also provide local estimates for more complex tools such as the combined Rossby wave and gravity wave diagnostics of Kinoshita and Sato (2013)." (line 8, page 16). Scientific conclusions are essentially absent. Again, it must be stressed that the results of the paper do not allow any conclusions with respect to propagation as only one time is considered and very simplifying assumptions are made.

We carefully revised the title, abstract and discussion considering the reviewer's suggestions. We concentrate in this paper on the diagnosis of GW appearance and hint on an upcoming publication building up on this initial results for further studies on propagation and generation.

Typos:
inhomogenous -> inhomogeneous (line 1 in Abstract)
artifical -> artificial (page 9, line 24)
". wave action .." -> ". Wave action âĂę" (page 8, line 28)
imhogeneous -> inhomogeneous (page 8, line 27)
All typos corrected.

A. Diagnosis of the Zimin Test Case

Diagnosis of the Zimin test case

V1R1 (25 Jan 2018 CZ) first draft

This is a technical report on the setup and application of “uwadi3figs.prj” which diagnoses the Zimin test case. This includes

- HIL (UWaDi): Hilbert transform as used with UWaDi
- STW (3DS): Stockwell transform which is also used in three dimensions
- SIN (S3D): Sinusoidal fit as is the base for three-dimensional sin-fit
- ACF (DIV, HDA): Auto-correlation function (so-called divergence method or Harmonic Divergence Analysis)

1 Setup for the second submission (October 2017)

For all the methods, we have used a box length of

$$L = 7.85 \tag{1}$$

The reason for this choice was oriented on experiences with ACF: For the maximum lag we allow for one fifth of the total length, and this should cover one wavelength

$$\lambda \leq \frac{L}{5} \tag{2}$$

and hence

$$L \geq 5\lambda \tag{3}$$

For the example we have used wavenumbers 4 and 9, which corresponds to a longest wavelength of

$$\lambda \leq 1.6 \tag{4}$$

and hence

$$L > 8.0 \tag{5}$$

While the wavepackets are placed at $x = 4.5$ and $x = 7.5$ their distance is 3 which is obviously smeared out with such a wide window. This is the major reason for the relative bad performance of the box-using methods SIN and ACF.

The choice of the box length is a matter of compromise between accuracy in space and wavenumber: While the spatial uncertainty is given by $\delta x = L$, the basic wavenumber is about $\delta k = 2\,\pi/L$ and hence

$$\delta x\;\delta k = 2\,\pi \tag{6}$$

Insofar the optimal box width is a matter of compromise and needs to be decided from case to case.

In the following we reconsider each diagnosis method and report on several sensitivity experiments.

2 Hilbert transform (HIL / UWaDI)

The Hilbert transform is a continuous method working without any box parameter. It returns values for every space point. Only some numerical trouble with the wavenumbers may occur for weak signals.

3 Stockwell transform

We start from the formulation of Wright *et al.* (2017) which is for the three-dimensional application. Reducing it back to our one-dimensional test case we retain the localization parameter (or dimensionless boxwidth factor) which is the width of the Gauss window

$$L = \frac{C_L}{f} = C_L\,\lambda \qquad (7)$$

In the paper, a C_L value of 0.25 has been used for analysis of AIRS data in the horizontal dimension and 0.1 for the vertical dimension. In the conventional formulations (Wright 2010) this parameter is included as 1.0. These different choices have been tested – see Figure 1. As expected, a large value of the boxwidth factor result in smeared distributions with a precise wavenumber, while a smaller value returns accurate amplitudes and more suspect wavenumbers. Based on these findings we choose a C value of 0.25 as we have done it for the UWaDi-2.

(a)	(b)

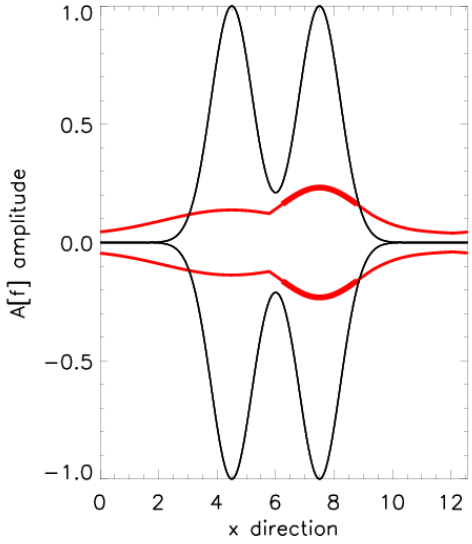
A[f] amplitude
x direction

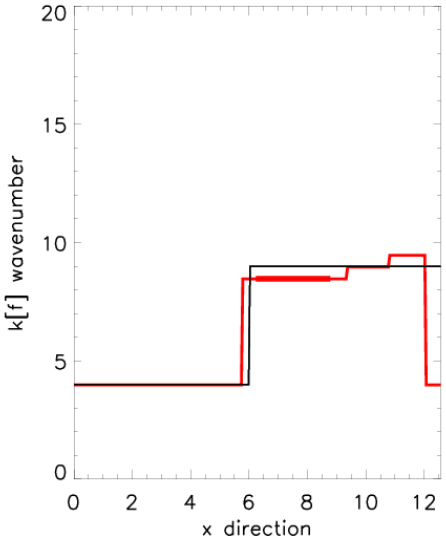
k[f] wavenumber
x direction

(c)

(d)

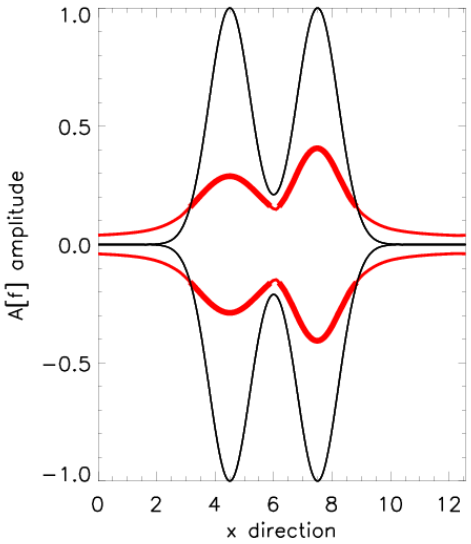
A[f] amplitude
x direction

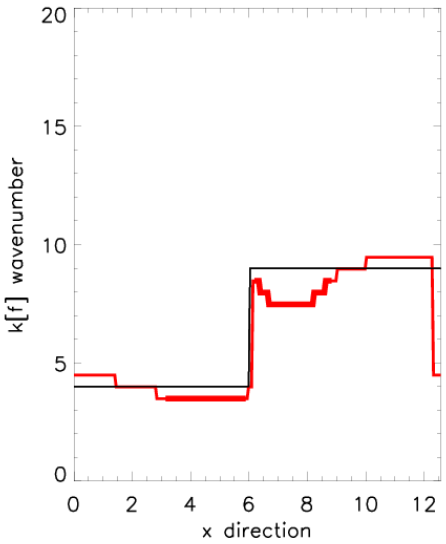
k[f] wavenumber
x direction

(e)

(f)

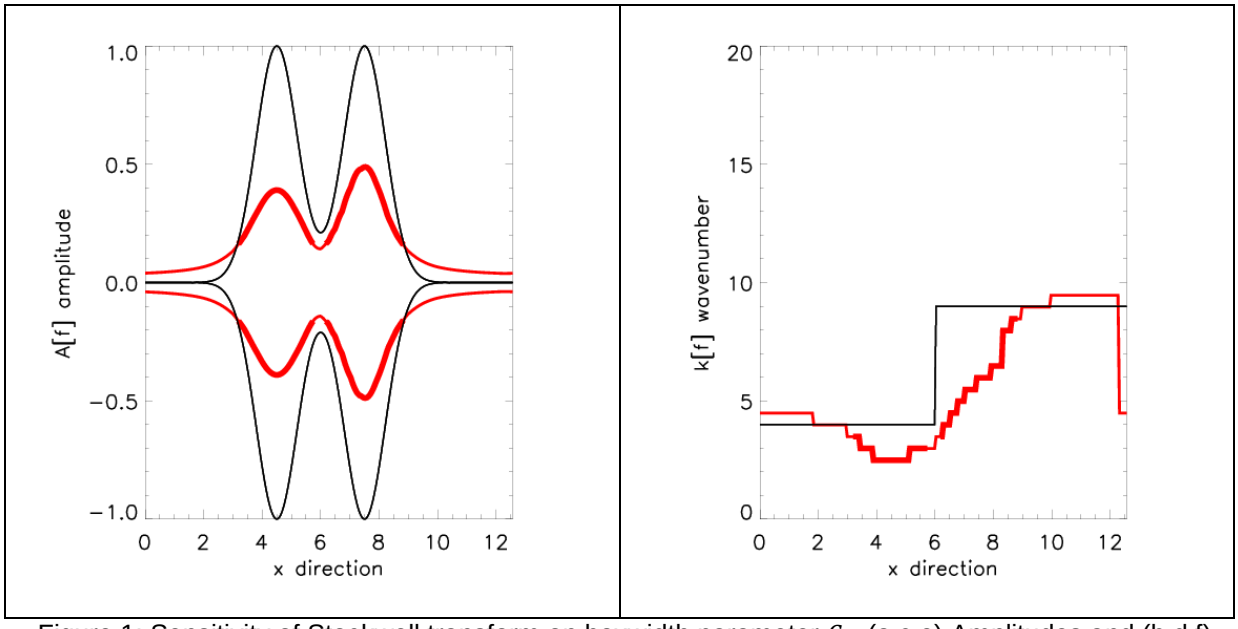

Figure 1: Sensitivity of Stockwell transform on boxwidth parameter C_L. (a,c,e) Amplitudes and (b,d,f) wavenumber for boxwidth parameters of (a,b) 1.0, (c,d) 0.25 and (e,f) 0.10. An amplitude factor of $C_A = 1.0$ is used.

Another issue mentioned by reviewer #1 is the amplitude correction factor (C_A). It was lined out by Wright *et al.* (2017) that "… the 3-D ST analysis exhibit significant amplitude reduction. This is due to fundamental limitations arising from the finite number of wave cycles present in any real wavepacket. While this problem is minor enough to be neglected for the 1-D ST (Wright, 2010), in the 3-D case it can reduce measured amplitudes by as much as 70% of their true value." We agree: the STW-amplitudes depend on the number of waves in a packet, but this is a matter which is different from dataset to dataset. Of course, one might introduce a correction factor but this is a bit covering an inherent disadvantage of STW. Because it is a local method, a too-small packet size may not suffice to average out the phases of the primary carrier wave. Additionally, any choice of an empirical amplitude correction destroys the analytical advantage of STW which is variance conservations: If the STW transform is integrated over space, the amplitude spectrum results exactly. Orienting on amplitude reductions by 40 – 70 % (Wright *et al.* 2017), we demonstrate the consequences on the power spectrum in Figure 2: The artificial change in amplitude destroys the variance conservation which manifests in the different curves in the right column. Note: The integral of the power spectrum equals the variance. That's why we decided to stay with $C_A = 1.0$.

(a)	(b)

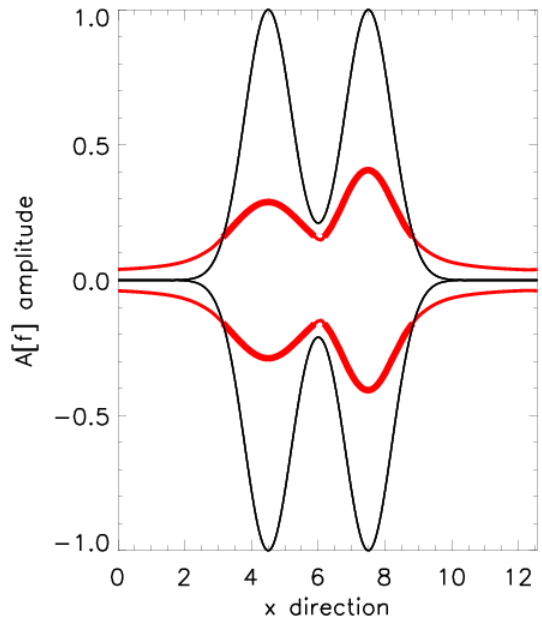
A[f] amplitude
x direction
1.0
0.5
0.0
−0.5
−1.0
0
2
4
6
8
10
12

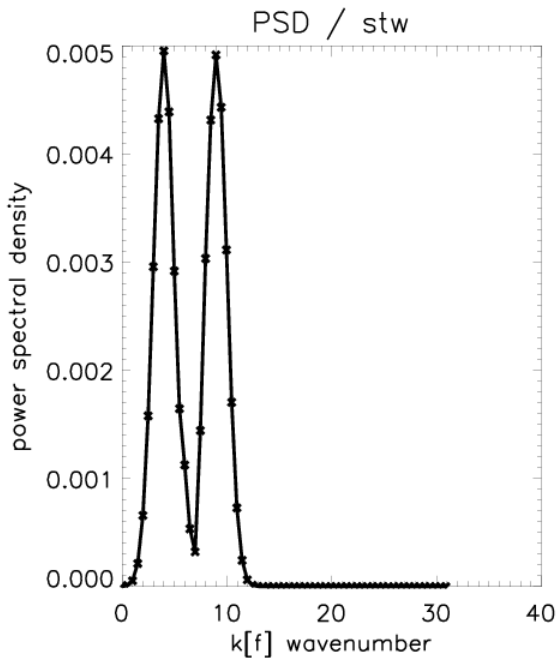
PSD / stw
power spectral density
k[f] wavenumber
0.005
0.004
0.003
0.002
0.001
0.000
0
10
20
30
40

(c)

(d)

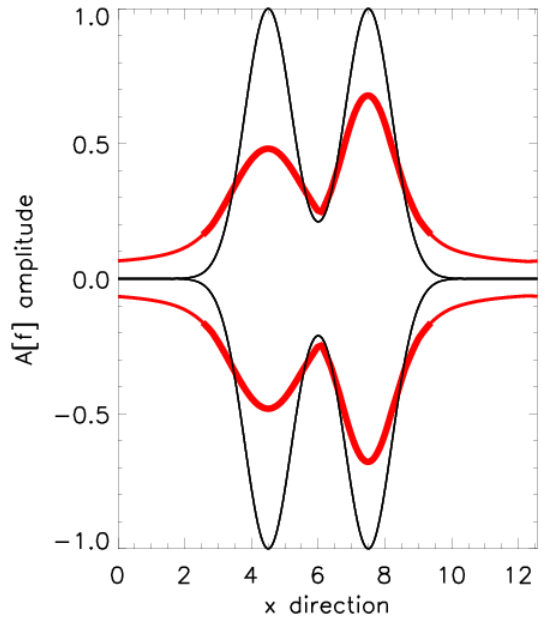
A[f] amplitude
x direction
1.0
0.5
0.0
−0.5
−1.0
0
2
4
6
8
10
12

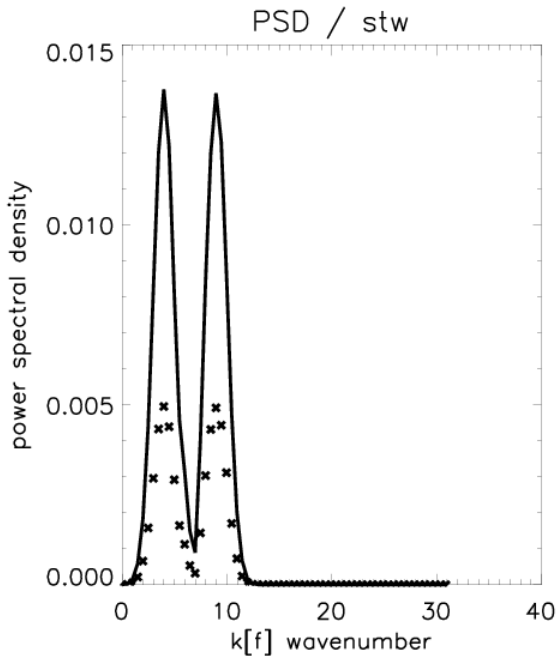
PSD / stw
power spectral density
k[f] wavenumber
0.015
0.010
0.005
0.000
0
10
20
30
40

(e)

(f)

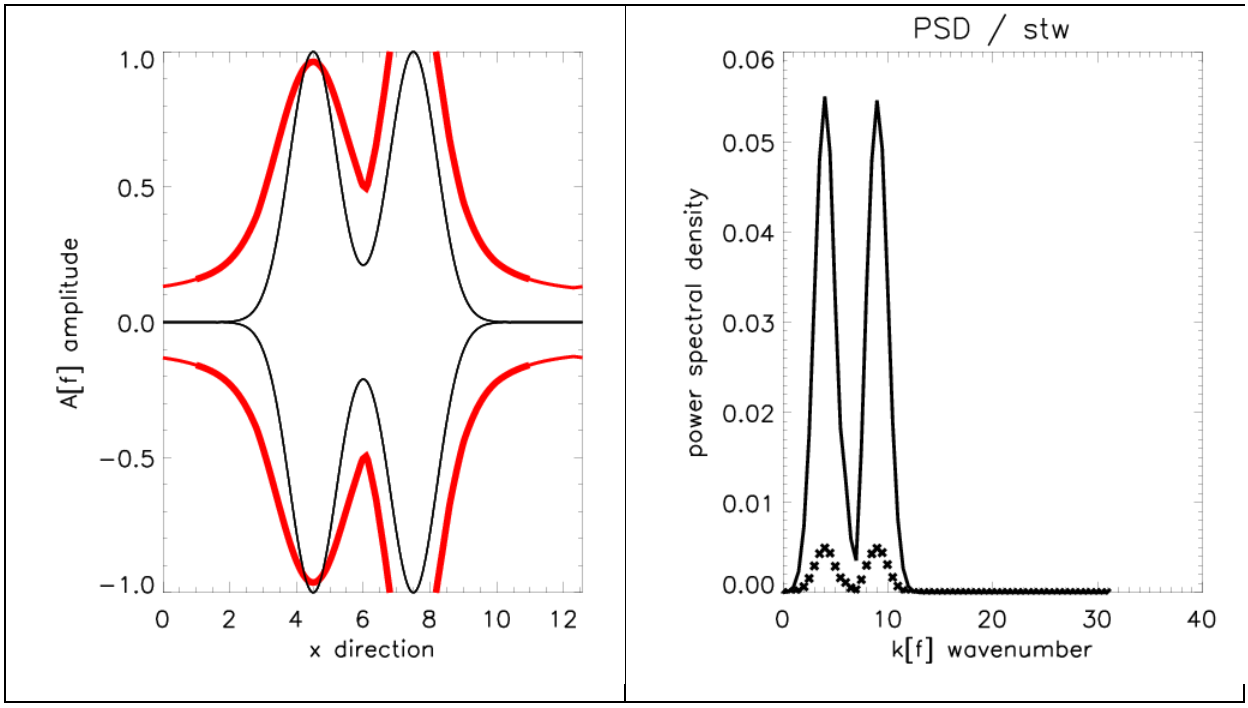

Figure 2: Sensitivity of Stockwell transform on amplitude correction C_A. Amplitudes (a,c,e) and power spectra (b,d,f; solid line: primary power spectrum, crosses: space-integrated Stockwell transform) for C_A factor of (a,b) 1.0, (c,d) $\frac{1.0}{0.6}$ and (e,f) $\frac{1.0}{0.3}$, each calculated with a boxwidth factor of $C_L = 0.25$

4 Sinusoidal fit (SIN / S3D)

The choice of $L_0 = 8.0$ for the UWaDi2 submission resulted in wide distributions smearing out the gap between the two wavepackets of the test case. As initial guess for the wavenumber fit we counted the Zeroes in the given box (N_{zero}) and used

$$k_{zero}^{(SIN)} = \frac{L_0}{N_{zero}} \tag{8}$$

For the initial guesses of the sinus and cosine amplitudes, we used half of the standard deviation for each in the hope, the IDL-LMFIT procedure would quickly converge. Several tests showed, that this was not really the case and the final result practically stayed with the initial wavenumber. For this procedure, we show the results for different box widths in Figure 3. The wide box ($L^{(SIN)} = 8.0$) smeared out amplitude and wavenumber, while the wavepackets amplitude and wavenumber were well separated with a medium box ($L^{(SIN)} = 1.5$) as suggested by reviewer #1. With the small box ($L^{(SIN)} = 0.5$) the amplitude quality remains good but we run into trouble with the wavenumber because our initialization did not find enough zero-crossings. Hence, the medium-size boxlength of 1.5 suits our purpose well. This is at

the one hand the period of the longer wave and also the half the distance between the wave packets.

(a)

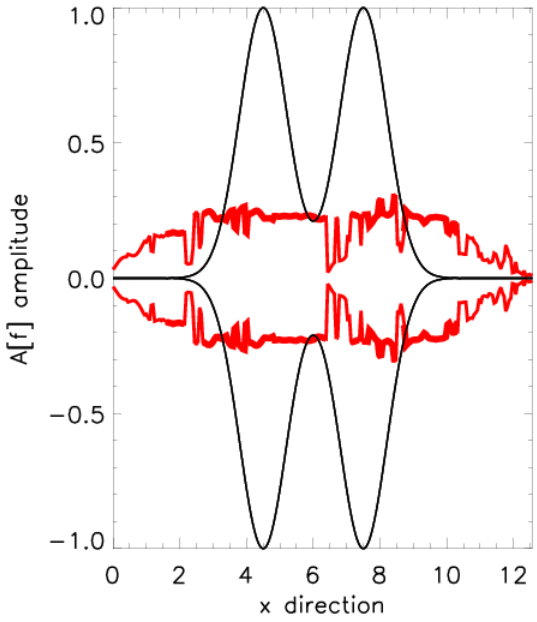

(b)

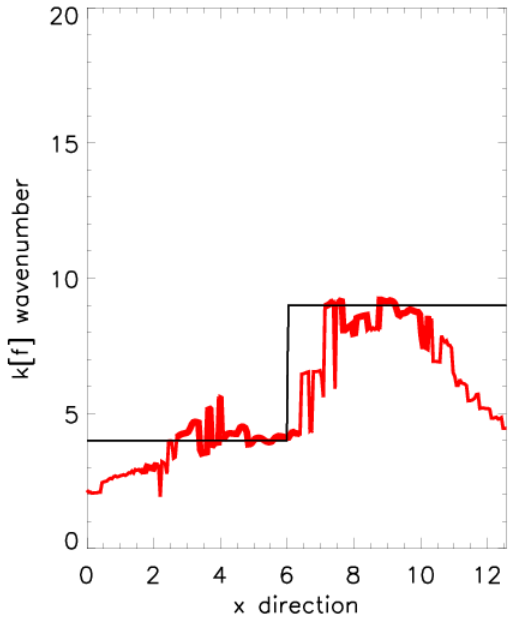

(c)

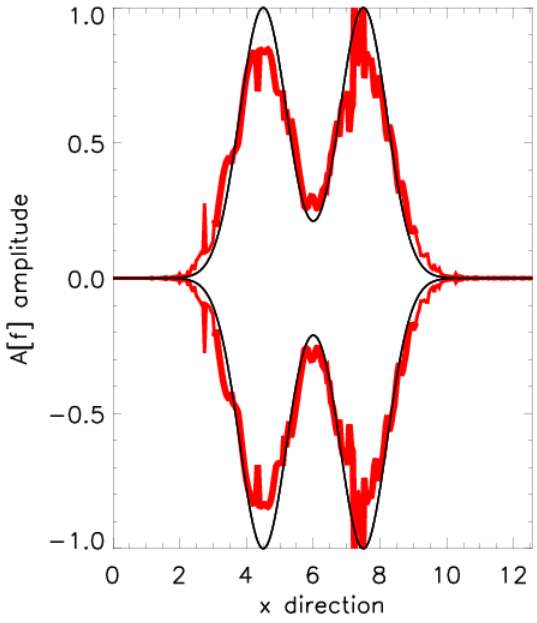

(d)

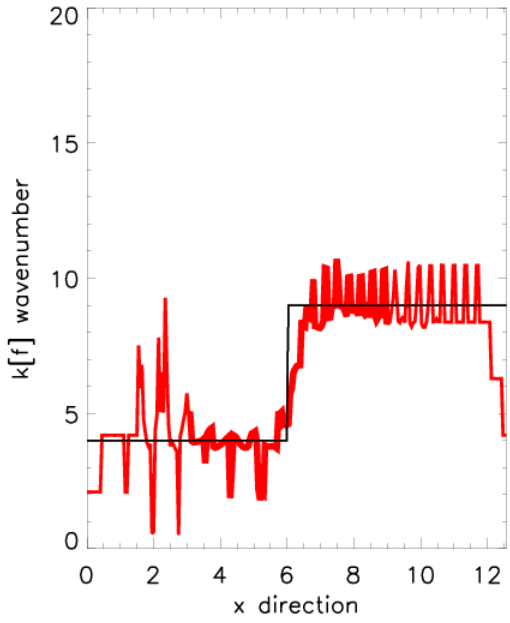

(e)

(f)

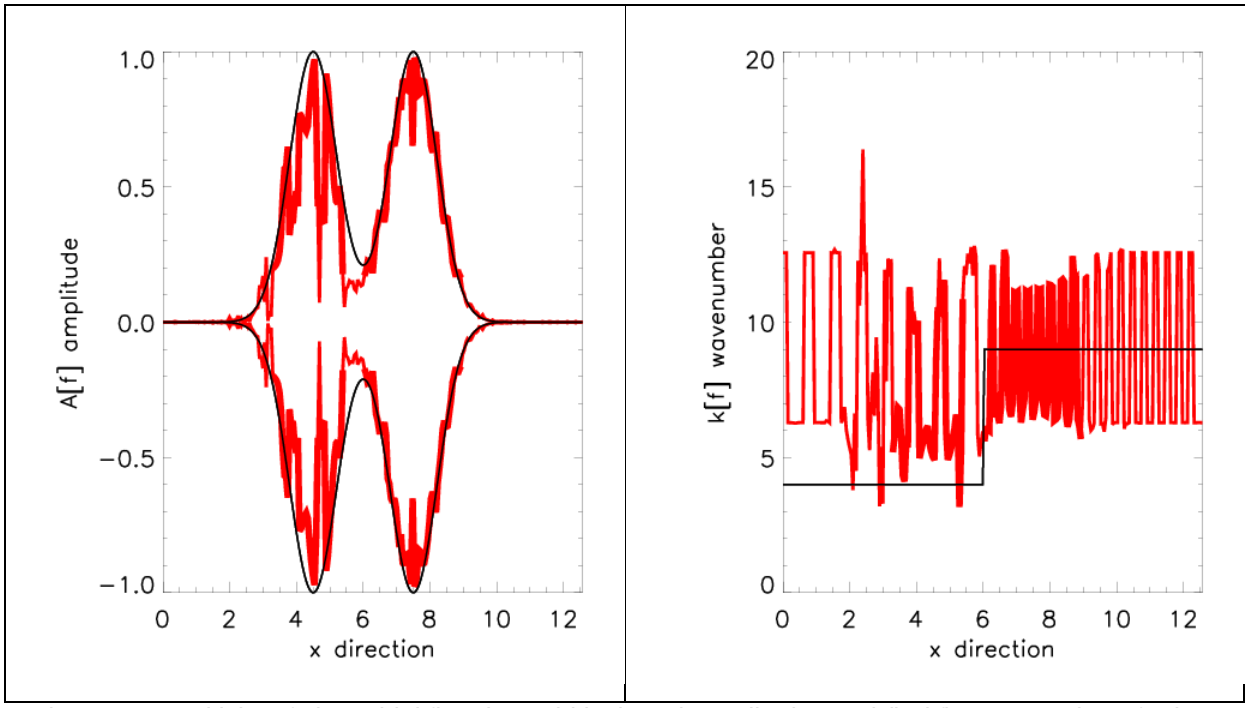

Figure 3: Sensitivity of sinusoidal fit to box width. (a,c,e) amplitudes and (b,d,f) wavenumbers for box width $L^{(SIN)}$ of (a,b) 8.0, (c,d) 1.5 and (e,f) 0.5. The IDL-LMFIT procedure was initialized with fixed amplitudes and the number-of-zero estimate for the wavenumber.

Next we compare different fitting procedures for the medium-size box of 1.5. Here, the cross-comparison with the FZJ procedures helped considerably – thanks to Peter Preusse at this point. We tried three further fitting methods (see Figure 4). The first alternative, labeled as SIN4, fixes the number-of-zero estimate for the wavenumber and fits the cosine and sine amplitudes. The amplitude (Figure 4a) is not very different from the one obtained with fitted k (Figure 3c), The wavenumber, however, appears slightly more stable (compare (Figure 4a with Figure 3d). The second alternative, labeled SIN5, picks the maximum of the power spectrum and fits the associated harmonic amplitudes. The amplitudes (Figure 4c) seem to be slightly smaller and the wavenumbers (Figure 4d) slightly smoother. Note the finite-size effect in the values: the first wavenumbers for a box of size 1.5 are 4.2 and 8.4, which are nearest to the theoretical values of 4.0 and 9.0. For the third alternative we directly used the IDL routine `sinfit_k` provided by Peter Preusse which searches the minimum in the chi-squared minimum in nested wavenumber intervals. As seen in Figure 4e and f, this method give the best results and will therefore be included in the new UWaDi submission.

(a)	(b)

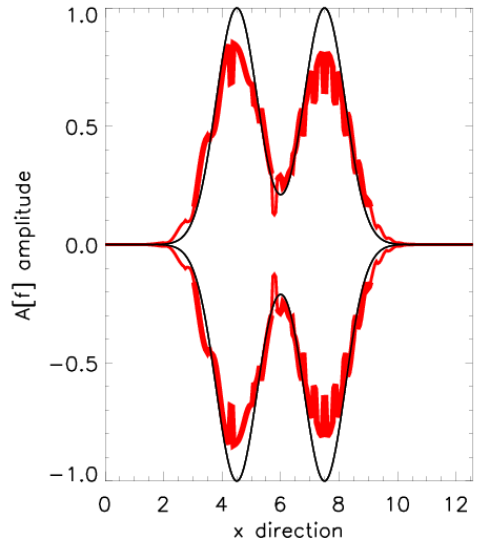
A[f] amplitude
x direction

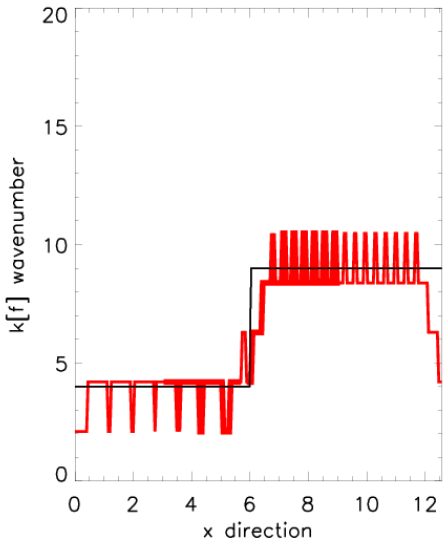
k[f] wavenumber
x direction

(c)

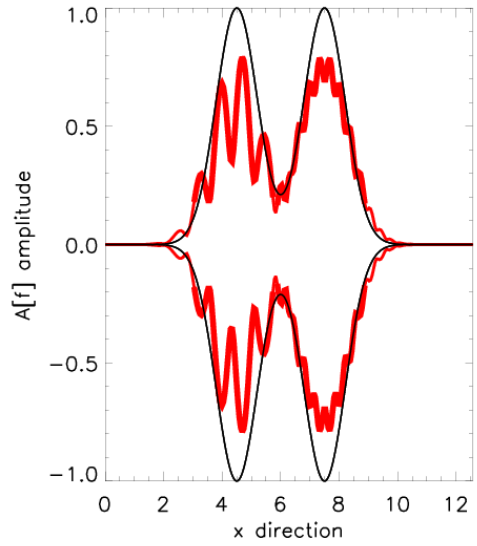
A[f] amplitude
x direction

(d)

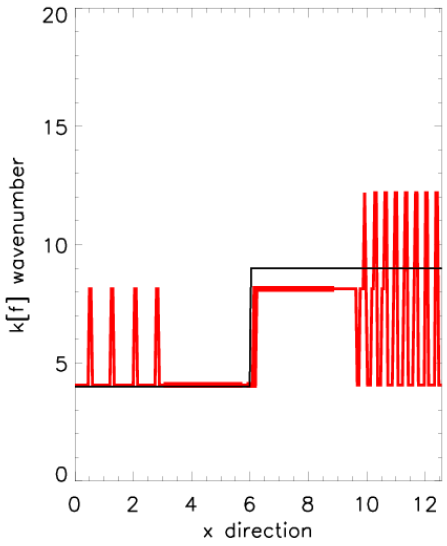
k[f] wavenumber
x direction

(e)

(f)

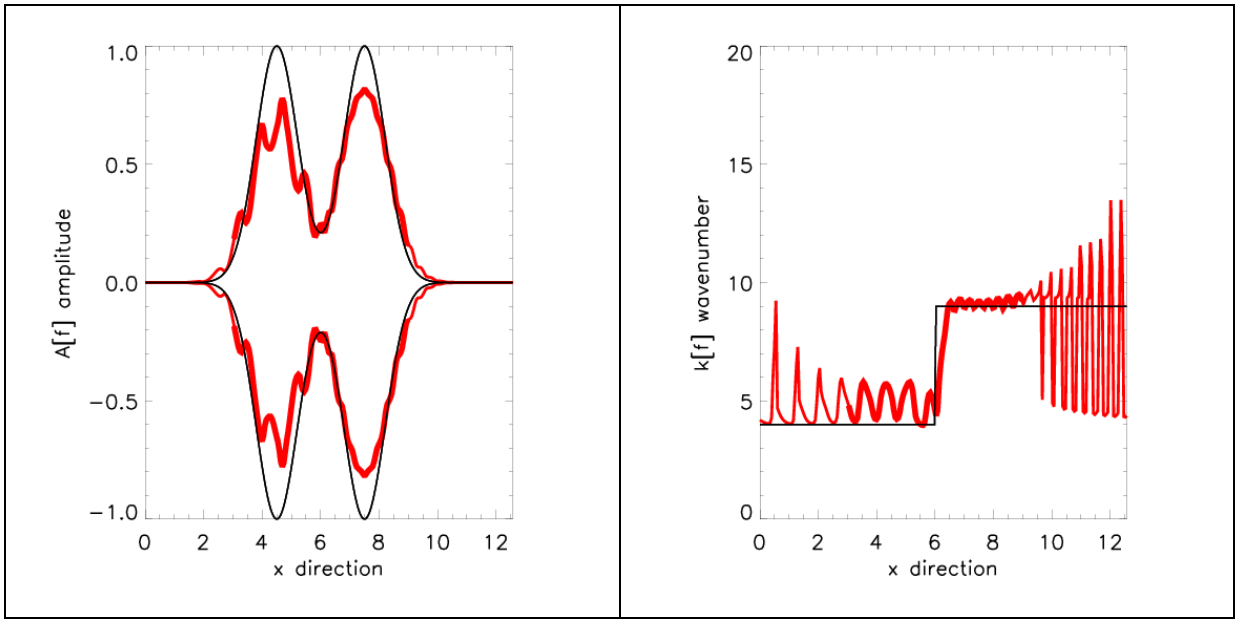

Figure 4: Sensitivity of sinusoidal fit to first guess. (a,c,e) amplitudes and (b,e,f) wavenumbers for (a,b) number-of-zero estimate (SIN4), (c,d) FFT maximum estimate (SIN5) and (e,f) chi-squared minimum estimate (SIN6)

Two remarks with regard to the figures provided in the review by Peter Preusse. There is a tiny difference between our SIN6 (Figure 4f) and his SINFIT (Figure 5f) which is due to the removal of a linear trend (which I did but he not). A minor difference is in the grid size (we are using $4\pi/252 = 0.050$ and he uses $4\pi/1000 = 0.013$) … A minor issue, anyway. The second remark is on his suggestion to embed the one-dimensional test case into three dimensions. For the analysis of these fields he uses a steepest-descent method to find the minimum in chi-squared (his `program s3d_uwadi_test_3d`). In view of his Figure 5, the wavenumber estimates for

$$
\begin{aligned}
f_1 &= \exp\left(-(z-4.5)^2\right)\cos(x+y+4z) + \exp\left(-(z-7.5)^2\right)\cos(x+y+9z) \\
f_2 &= \exp\left(-(z-4.5)^2\right)\cos(x+y+4z) + \exp\left(-(z-7.5)^2\right)\cos(x-y+9z) \qquad (9) \\
f_3 &= \exp\left(-(z-4.5)^2\right)\cos(4z) + \exp\left(-(z-7.5)^2\right)\cos(9z)
\end{aligned}
$$

are smoother when three dimensions (f_1 and f_2) are used. I could imagine that the search algorithm converges more stable when the “added” waves in x and y direction vary over one wavelength and provide more or less a certain phase average. If convergence is searched without them (f_3), these phases influence the result. These rapid changes in wavenumber are a partly reduced when a linear trend is eliminated (compare SINFIT in Figure 5f with SIN6 in Figure 4f). That’s why we use the

detrended nested-interval 1.5-boxlength estimates ($L^{(SIN)} = 1.5$) in the third submission.

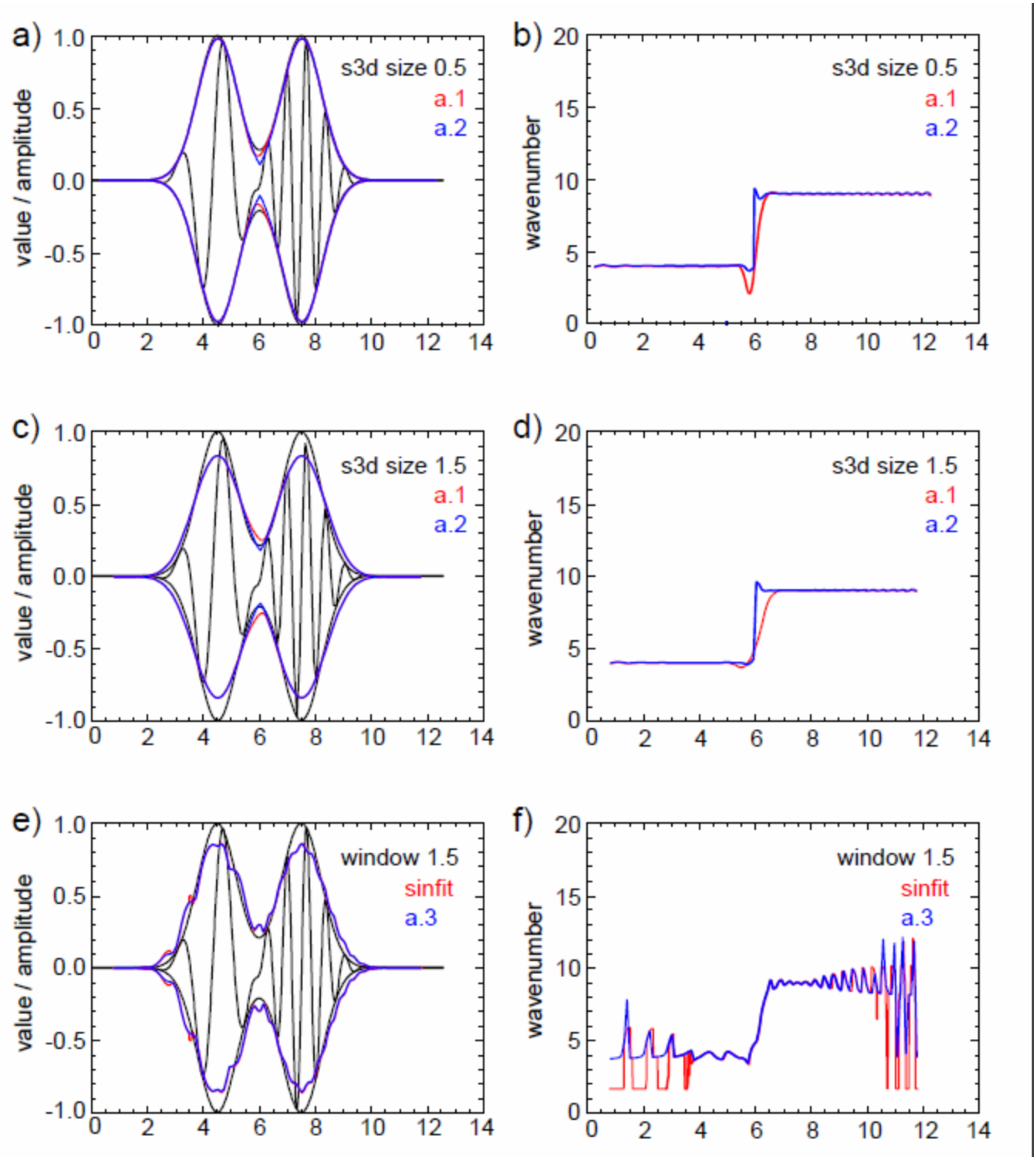

Figure 5: Sinusoidal fits provided by Peter Preusse. (a,c,e) Amplitudes and (b,d,f) wavenumbers for (a,b) S3D fit with window size 0.5, (c,d) S3D fit with window size 1.5 and (e,f) S3D and SINFIT with window size 1.5

5 Auto-correlation function (ACF / DIV, HDA)

The analysis of the auto-correlation function, as it was used with the divergence method (DIV) in (Zülicke & Peters 2006, 2008) or as the harmonic divergence analysis (HDA) in (Mirzaei *et al.* 2014; Mirzaei *et al.* 2017), aims to find the first zero-crossing in a phase-independent estimate of a cosine function. As lined out in section 1, the conservative box length is be about 8 which smears out both amplitude and wavenumber as shown in Figure 6a and b. Using a slightly narrower box of 3.0 width, the gap between the two wave packets is still not resolved but the wavenumbers show a more narrow transition between the two (Figure 6c,d). The rapid wavenumber oscillations increase and the left wavenumber estimation fails completely for a narrow box as used above (1.5). Only the amplitudes separate the two wave packets well (Figure 6e,f). That's why we choose a box width of $L^{(ACF)} = 3.0$ for the third UWaDi submission.

<table>
<tr><td>(a)
 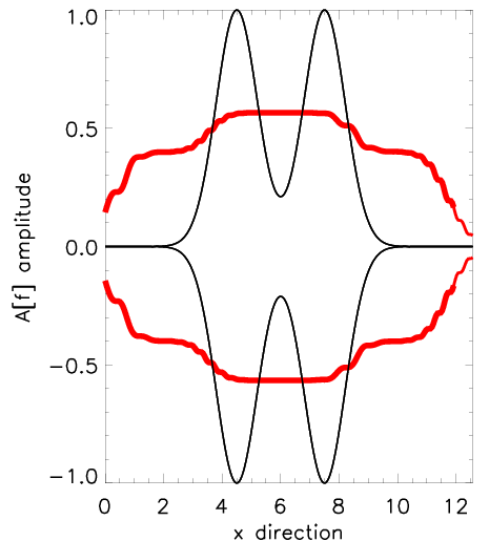
</td><td>(b)
 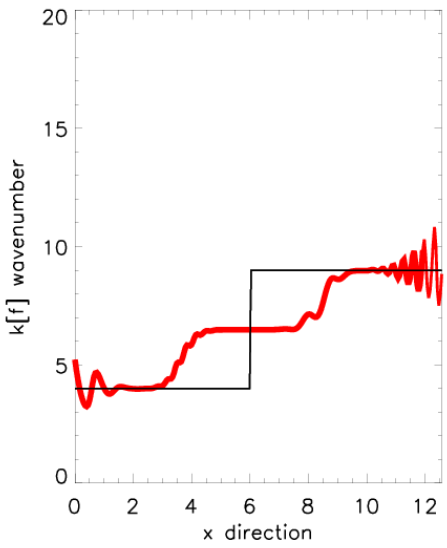
</td></tr>
<tr><td>(c)</td><td>(d)</td></tr>
</table>

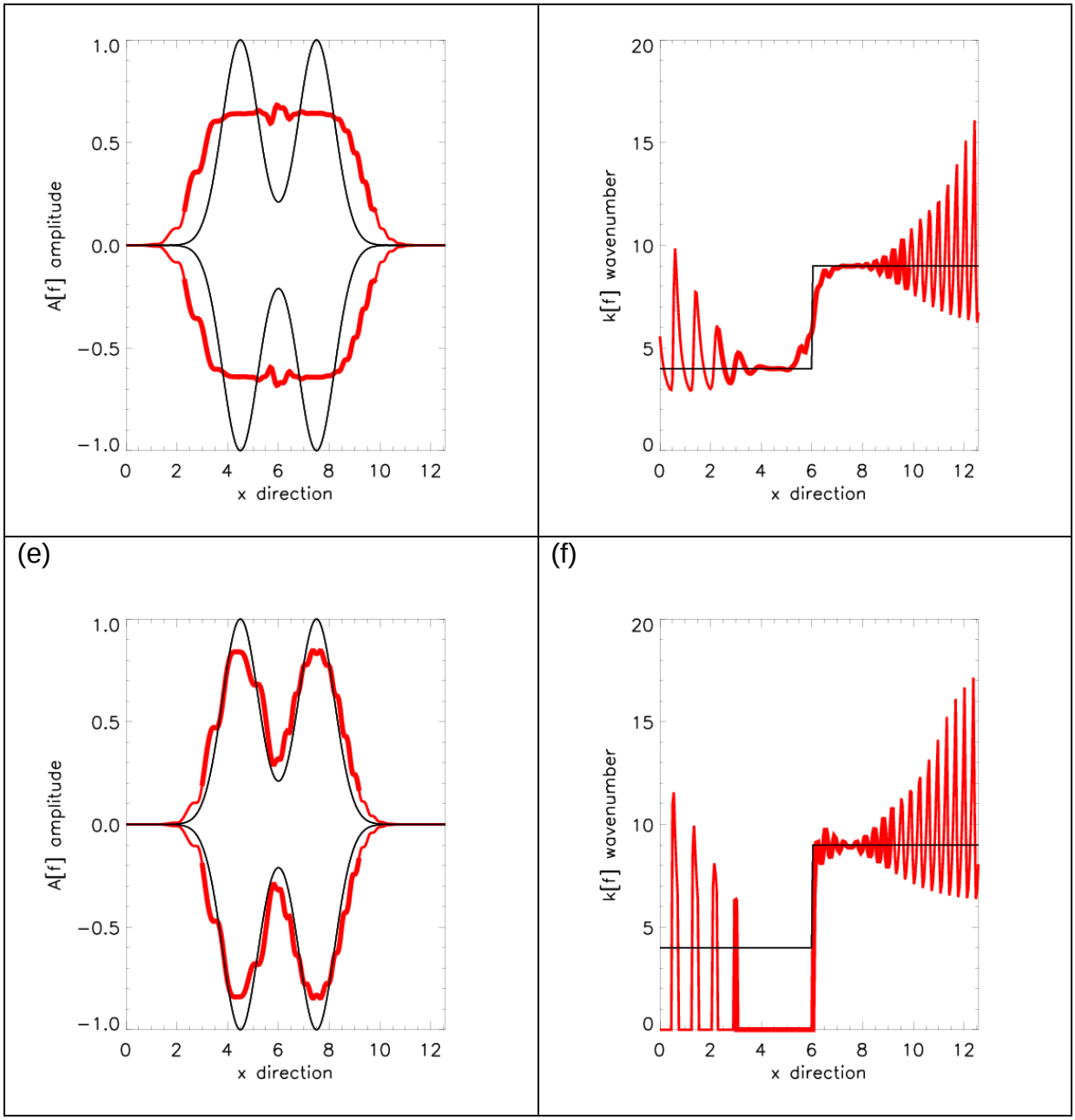

Figure 6: Sensitivity of the auto-correlation-function method on the box width. (a,c,e) Amplitude and (b,d,f) wavenumber for a box width of (a,.b) 7.86, (c,d) 3.0 and (e,f) 1.5.

6 Summary and conclusion

For the method intercomparison we follow the advice of the reviewer 1 (Peter Preusse). While we used in the second submission a relatively wide box ($L = 8.6$) for SIN and DIV to enhance the difference between box-based and box-independent methods, we relax this approach and allow for finer adjusted box width now. In particular we found relatively robust results after trend elimination for the choices $L^{(SIN)} = 1.5$ and $L^{(ACF)} = 3.0$. We could attribute also a kind of box length to the STW

method, which was fixed with the factor $C^{(STW)} = 0.25$ to $L^{(STW)} = 0.39$ for the longest test wave. No of such box length needs to be specified for HIL which actually delivered the most stable estimates for amplitude and wavenumber.

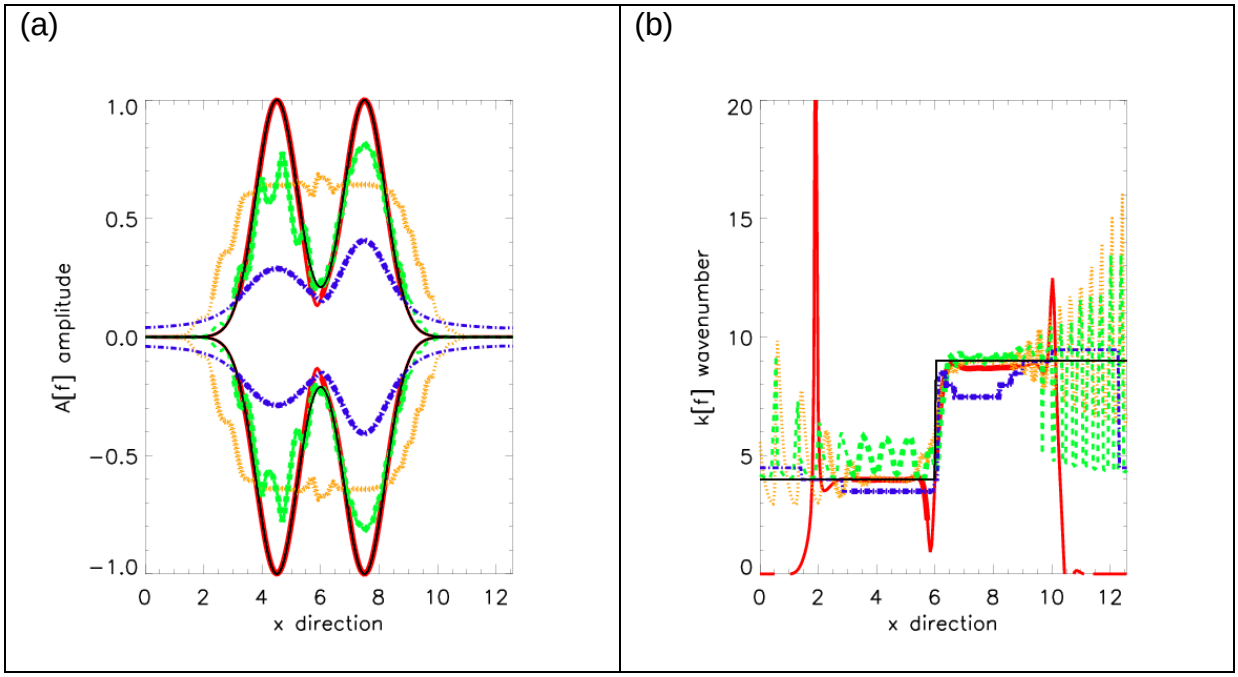

Figure 7: Method intercomparison. (a) Amplitude and (b) wavenumber of (solid red) HIL, (dash-dotted blue) STW, (dashed violet) SIN and (dotted orange) ACF. Bold lines mark valid estimates.

Reference

Mirzaei, M., A. R. Mohebalhojeh, C. Zülicke & R. Plougonven, 2017: On the quantification of imbalance and inertia-gravity waves generated in numerical simulations of moist baroclinic waves using the WRF model. *J. Atmos. Sci.* **74**: 4241-4263, doi:10.1175/jas-d-16-0366.1.

Mirzaei, M., C. Zülicke, A. R. Mohebalhojeh, F. Ahmadi-Givi & R. Plougonven, 2014: Structure, energy and parameterization of intertia-gravity waves in dry and moist simulations of a baroclinic wave life cycle. *J. Atmos. Sci.* **71**: 2390 - 2414, doi:10.1175/JAS-D-13-075.1.

Wright, C. J., 2010: Detection of stratospheric gravity waves using HIRDLS data PhD, Oxford.

Wright, C. J., N. P. Hindley, L. Hoffmann, M. J. Alexander & N. J. Mitchell, 2017: Exploring gravity wave characteristics in 3-D using a novel S-transform technique: AIRS/Aqua measurements over the Southern Andes and Drake Passage. *Atmos. Chem. Phys.* **17**, 13: 8553-8575, doi:10.5194/acp-17-8553-2017.

Zülicke, C. & D. H. W. Peters, 2006: Simulation of inertia-gravity waves in a poleward breaking Rossby wave. *J. Atmos. Sci.* **63**, 12: 3253 - 3276, doi:10.1175/JAS3805.1.

Zülicke, C. & D. H. W. Peters, 2008: Parameterization of strong stratospheric inertia-gravity waves forced by poleward breaking Rossby waves. *Mon. Wea. Rev.* **136**, 1: 98 - 119, doi:10.1175/2007MWR2060.1.

B. Revised Manuscript

~~Diagnosis of Local Gravity Wave Properties during a Sudden Stratospheric Warming~~A novel method for the extraction of local gravity wave parameters from gridded three-dimensional data: description, validation and application

Lena Schoon[1] and Christoph Zülicke[1]

[1]Leibniz-Institute of Atmospheric Physics, Schlossstrasse 6, 18225 Kühlungsborn, Germany

Correspondence to: Lena Schoon (schoon@iap-kborn.de)

Abstract. ~~The selective transmission of gravity waves through an inhomogeneous mean flow is investigated.~~ For the local diagnosis of wave properties we develop, validate and apply a novel method which is based on the Hilbert transform~~and~~. It is named "Unified Wave Diagnostics" (UWaDi). ~~Thus, i~~It provides ~~wave properties~~ the wave amplitude and three-dimensional wave number at any grid point for ~~any wave-containing data~~gridded three-dimensional data. UWaDi is validated for a synthetic test case comprising two different wave packets. In comparison with other methods, the performance of UWaDi is very good with respect to wave properties and their location. For a first practical application of UWaDi, a minor sudden stratospheric warming on 30 January 2016 is chosen. Specifying the diagnostics ~~on~~for hydrostatic inertia-gravity waves in analyses from the European Centre for Medium-Range Weather Forecasts, we ~~confirm~~detect local~~ly different transmission~~ appearance of gravity waves throughout the middle atmosphere. ~~These are~~It is ~~interpreted~~discussed in terms of ~~columnar~~ vertical propagation using the ~~additionally~~ diagnosed local amplitudes and wave numbers. We also note some hint on local inertia-gravity wave generation by the stratospheric jet from the detection of shallow slow waves in the vicinity of its exit region.

1 Introduction

The importance of gravity waves (GWs) for the dynamics of the Earth's atmosphere is without controversy. They influence dynamics from planetary scales to turbulent microscales and play an important role in the middle atmosphere circulation (Fritts and Alexander, 2003). The GWs typically appear as packets localised in space and time. Hence, it is desirable to diagnose them locally as precise as possible. Here, we want to introduce a new method named "Unified Wave Diagnosis" (UWaDi). ~~The method~~It provides phase-independent local wave quantities like amplitude and wave number without any prior assumption. In the following, we ~~want to~~ develop, validate and apply the~~is~~ novel method. The application concentrates on the analysis of GWs for locally varying background wind conditions in the winter 2015/16.

In the past, several methods were developed to estimate wave properties like amplitudes and wave number vectors. All of them have to deal with the fact that the data sampling procedure influences the results. A common approach to obtain vertical wave numbers and GW frequency of high-passed filtered wind fluctuations are Stokes parameters (Vincent and Fritts, 1987). This

method is based on the~~definition of~~ polarisation relations and works for single-column measurements. It provides the wave properties in preselected vertical height sections of finite lengths. Next to its original application on radar measurements it is used for radiosonde data (Kramer et al., 2015). A supplement to this method named DIV was introduced by Zülicke and Peters (2006). It determines the dominating harmonic wave in a box from the first zero-crossing of the auto-correlation function. The maximal de~~e~~tectable wavelength is restricted by the box size. The analysed quantity is the horizontal divergence to get the ageostrophic flow without numerical filtering. A further technique is based on sinusoidal few wave fits (~~S-3D~~S3D) (Lehmann et al., 2012). This method was created for the analysis of binned data from remote sensing ~~(Ern and Preusse, 2012; Ern et al., 2014)~~(Ern et al., 2017; Krisch et al., 2017) but is also applicable to model data (Preusse et al., 2014). The first ~~two~~ modes with highest variance are taken from a fit that minimises the variance-weighted squared deviations over all points in a finite analysis box. Only a small number of sinusoidal curves are fitted and there might remain uncovered variances in the analysis volume. ~~All t~~These methods have in common, that the analysed spatial scales are dependent on the predefined analysis box size and the assumption of spatial homogeneity of the wave field in these boxes is essential. Nevertheless, these methods are superior to a classic Fourier transform in that point that they allow to search for waves with bigger wavelengths than the box size. ~~Here, we want to develop a method which provides wave parameters locally, meaning at each grid point.~~

Another three-dimensional spectral analysis method is the 3D S~~T~~tockwell-transform (~~3D-ST~~3D ST) (Wright et al., 2017). This method is capable of analysing the full range of length scales sampled in satellite data and is not restricted to fixed box sizes. At every grid point, a local wave spectrum is estimated using a window function of frequency-dependent width. ~~With this method available local wave quantities are wave vectors, amplitudes, phase and group velocities, temporal frequencies and momentum fluxes. However, directions of vector quantities have to be fixed by separate assumptions. Both,S-3D~~S3D and ~~3D-ST~~3D ST assume homogeneity inside the analysis box. Furthermore, they use a small number of the most-prominent waves for the estimation of variances. This leaves some variance unattributed and hence means a loss of information. ~~look for the largest spectral amplitude to calculate the wave quantity at the respective box point. This might lead to a loss of information, in any case the estimated variance is too small.~~We search for a method which detects the full variance in each data point.

With UWaDi we find the dominating wave with the Hilbert transform at every data point. It makes data binning into finite analysis boxes redundant. The calculation of wave quantities at every grid point is computationally cheap. There is no need of assuming homogeneity and no restriction to detectable wavelengths besides the Nyquist wavelength. Here, the method ~~and~~ is developed to work with three-dimensional equally-gridded data. In general, the Hilbert transform can be applied to data of any dimensionality. Wave properties such as the amplitude and wave number are estimated phase-independently while all variance is attributed to one wave mode. Every variable including any kind of wave-like structure~~is analysable~~can be diagnosed.~~and preselection of modes is avoided.~~ Zimin et al. (2003) used the method to obtain the envelope of a train of Rossby waves in one dimension. A supplement was made for waves not in-line with grids by an extension of the formulation to stream lines to obtain quasi-one-dimensional wave packets (Zimin et al., 2006). ~~Kinoshita and Sato (2013)~~(Sato et al., 2013) provide a three-dimensional application on Rossby and GWs. Glatt and Wirth (2014) use the Hilbert-transform to identify Rossby wave trains on a longitude-time plane and introduce their approach as an "objective identification method". Our method ~~comes up with an enhancement for three dimensions~~focuses on the local site of GW appearance and the additionally provision of the wave

number in every dimension. The latter ~~which~~ was not presented before. We aim to cover the retrieval of local wave properties from arbitrarily orientated wave packets. Amplitude and wave number are ~~sampled~~returned on the same grid as the input data. After the mathematical description of the method and how it is implemented, it will be validated with synthetic data ~~sets~~ to demonstrate its quality in comparison with other methods.

For a demonstration of a practical application in geophysical context, we will investigate GWs. Their sources are usually found in the troposphere where waves are generated by flow over orography, by convection, frontal systems and jet imbalances. These waves propagate upwards with increasing amplitudes and break in the middle atmosphere where they deposit their momentum to the background flow. Strong influence is exerted on global circulation patterns in the mesosphere as well as in the stratosphere (Holton, 1983; Garcia and Solomon, 1985). GWs play crucial roles in the modulating of the quasi-biennial oscillation (QBO) and the Brewer-Dobson circulation (Dunkerton, 1997; Alexander and Vincent, 2000; Ern et al., 2014). Another stratospheric phenomenon where GWs play a role are sudden stratospheric warmings (SSW). For this phenomenon, a~~A~~ variety of definitions exists (Butler et al., 2015), but the most common one is given by the World Meteorological Organization stating that an SSW is characterised by a reversal of the 60° N to 90° N-temperature gradient. Major warmings are associated with a wind reversal at 10 hPa and 60° N; minor SSWs (mSSWs) with a wind deceleration at 10 hPa and 60° N, where the prevailing westerlies are not turned into easterlies. ~~Even though~~While planetary waves are the most important drivers of SSWs (Andrews et al., 1987), GWs are affected by the differing background wind conditions during SSWs and are suspected to modulate the polar vortex in the postwarming phase of an SSW (Albers and Birner, 2014). The ~~coupling~~behaviour of GWs ~~with~~and planetary waves during an SSW was investigated by simulations and different measurement techniques. ~~Restricted to zonal mean wave properties, local eastward propagating GWs can only be estimated by anomalies in horizontal divergence fields. Nonetheless,~~It was found that these GWs are, next to selective transmission, ~~assigned to GW emission and~~subjects of variable sources including unbalanced flow adjustment (Yamashita et al., 2010; Limpasuvan et al., 2011). We are interested in the longitude-dependent transmission of GWs during an SSW. Pioneering work was done by Dunkerton and Butchart (1984). They analysed model data and found that selective transmission of GWs during an SSW is dependent on longitude according to the planetary wave structures. Therefore, regions where vertical wave propagation is inhibited exist as well as regions where waves can propagate up to the mesosphere. The analysis of Dunkerton and Butchart (1984) was restricted to parameteri~~z~~sed GWs of the "intermediate range", that they defined between 50 km and 200 km. They state that it remains unclear, in what kind GWs of larger scale will act during SSWs. A study on a self-generated SSW in a model showed that GWs reverse the circulation in the mesosphere-lower thermosphere during an SSW by altering the altitude of GW breaking. This altitude is highly dependent on the specification of GW momentum flux in the lower atmosphere (Liu and Roble, 2002; Zülicke and Becker, 2013). ~~This is where our analysis sets in.~~In the UWaDi application, ~~W~~we want to diagnose the appearance of GWs precisely in space and give ~~an~~ first interpretations using the information on their changing amplitude and wave number in local vertical profiles. ~~For that purpose, we will use UWaDi with a GW-specific diagnostic.~~

The northern winter 2015/16 brought up several interesting features, including ~~several issues~~specific GW patterns ~~of GW behaviour~~. The beginning of the winter was characterised by an extraordinarily strong and cold polar vortex driven by a deceleration of planetary waves in November/December 2015 (Matthias et al., 2016). Thereinafter, for the end of that winter a

record Arctic ozone loss was expected (Manney and Lawrence, 2016). Furthermore, the extraordinarily polar vortex caused a southward shift of planetary waves leading to anomalies in the QBO (Coy et al., 2017). Inbetween, a joint field campaign of the research ~~projects METROSI, GW-LCYCLE 2 and PACOG~~units ROMIC (METROSI, GW-LCYCLE2) and MS-GWaves (PACOG) took place in Scandinavia in January 2016. Stober et al. (2017) found a summer-like zonal wind reversal in the upper mesosphere lasting until the end of January 2016, leading to different GW filtering processes in the mesosphere compared to usual winter-like wind conditions. During the field campaign first tomographic observations of GWs by an infrared limb imager provide a full three-dimensional picture of a GW packet above Iceland (Krisch et al., 2017). Additionally, a remarkable comparative study shows that forecasts of the current operational cycle (41r2) of the European Centre for Medium-Range Weather Forecasts (ECMWF) Integrated Forecast System (IFS) shows good accordance with space-borne lidar measurements while picturing large-scale and mesoscale wave structures in polar stratospheric clouds (Dörnbrack et al., 2017). We choose the mid-winter of 2016 for a~~n~~ first application of UWaDi because it is very well sampled with observations of GW properties. ~~Hopefully, we~~We intend to ~~may~~provide additional impulses to the evaluation of observations and start with a study of ECMWF analyses.

~~In particular, UWaDi requires regular gridded data. Assimilated data products from ECMWF~~These gridded data are suitable to analyse the local ~~phenomena~~appearance and their coupling as ~~they~~the analyses resolve essential parts of GW dynamics in the stratosphere.~~Even the T799 resolution gives proof of correct GW appearance in the stratosphere.~~ Validation studies with satellite measurements point out that ECMWF analyses capture~~s~~ GWs well in the mid- and high-latitudes (Yamashita et al., 2010; Preusse et al., 2014). ~~The improved T1279 resolution yields to a bigger portion of resolved GWs in ECMWF data. Validation studies with measurements show that~~ Especially mid-latitude GWs are captured well being driven by orographic and jet-stream associated sources (Shutts and Vosper, 2011; Jewtoukoff et al., 2015). Our approach concentrates on fields of horizontal divergence of ECMWF IFS data. The horizontal divergence counts for a dynamical indicator for GWs (Plougonven et al., 2003; Zülicke and Peters, 2006). Its magnitude was found to correlate with temperature anomalies induced by mountain waves (Dörnbrack et al., 2012; Khaykin et al., 2015). ~~We concentrate on vertical propagation only, highlighting selective transmission.~~ In this study we concentrate on vertical profiles of GW appearance to give a first impression of the functionality of this method. Studies arguing the restrictions on vertical-only propagation can be found in Yamashita et al. (2013), Kalisch et al. (2014) and Ehard et al. (2017). We point out that meridional propagation of GWs can play an important role for the analysis of the deposition of GW drag from the stratosphere up into ~~in~~ the mesosphere. Oblique propagation of GWs may even redistribute the selective transmission of GWs in the upper troposphere and lower stratosphere (e.g. Krisch et al., 2017). ~~As we give an idea of GW propagation in the upper troposphere and stratosphere we concentrate on vertical propagation and are aware of the possibility of GW entrainment of strong winds.~~ These are interesting phenomena which require a detailed analysis of the propagation of localised wave packets. Here, the authors focus on the introduction of the novel method and give first preliminary scientific results from the demonstrative application. We show locally diagnosed GW properties and give some hints on physical interpretation. A full three-dimensional spatial-temporal analysis of GWs during the SSW 2015/16 goes beyond the scope of this paper and will be made subject of subsequent publications.

The paper is organised as follows. After providing a step-by-step introduction and validation of the novel method in Section 2, we give a short overview of the estimation of wave quantities for synthetic data and describe the analysis data. In Section 3 we show our results for the application on the mSSW on 30 January 2016 where we study ~~local~~ longitude-depending GW ~~generation and propagation~~ appearance. The discussion of our results in Section 4 is followed by the Summary and Conclusion (Sec. 5).

2 Method and Data

In this section we develop and validate an algorithm to extract wave parameters from gridded three-dimensional data. For local diagnosis of waves, phase-independent estimates of wave amplitudes as well as the wave vector are essential. For this, we employ the Hilbert transform ~~(Von Storch and Zwiers, 2001)~~(e.g. Von Storch and Zwiers, 2001). The Hilbert transform shifts any sinusoidal wave structure by a quarter phase, i.e. turning a sine into a cosine. By constructing a new complex-valued data series ~~number~~ consisting of the original field as real part and its Hilbert transform as the imaginary part, the absolute value is always the amplitude (square root of squared real and imaginary part). The amplitude is independent of the phase of the wave and the wavelength of the underlying oscillation and there is no need of any explicit fitting of a particular wave. In addition, the absolute wave number in all three dimensions is determined from the phase gradient. The only requirement of the method to work is that the data contain any harmonic component. This makes up the unified character of the wave diagnostics.

2.1 Step-by-step outline of the method

In the following we introduce UWaDi by a step-by-step outline. Further, we validate it with a well-defined test wave packet in comparison with other methods. In general, UWaDi is a script package which allows the user to steer data preprocessing, the main wave analysis and data plotting, from a set of namelists. ~~This package is coded in open source software such as NCL and Fortran. Its multi-purpose applicability on a set of arbitrary waves, e.g. gravity waves or planetary waves, defines its unified character.~~

1. ~~Firstly, the three-dimensional gridded data is preprocessed.~~ UWaDi requires data from equidistant grids. ~~Horizontally, the grids are equidistant if they are provided on a regular latitude-longitude grid.~~For the ECMWF analyses on a longitude-latitude grid, the ~~The~~ latitude-dependence of grid distance is taken into account by determining the longitudinal grid distance by $dx = 2\pi r_\theta \frac{\gamma}{360}$ where $r_\theta = R\cos(\theta)$ is the latitude-depending earth radius ($R = 6371\mathrm{km}$ - earth radius; θ - latitude [°]) and γ denotes the resolution of the gridded input data (e.g. $\gamma = 0.36°$). ~~Vertical interpolation from model levels to equidistant height levels is performed by associating constant heights with pressure levels.~~

2. To retrieve vertical equidistant levels firstly, the hybrid levels of the ECMWF data are transformed to pressure levels. Secondly, these pressure levels are assigned to equidistant height levels. For this purpose, we assume hydrostatic conditions

and consider the surface geopotential and pressure as well as temperature and humidity. Both steps are performed with the help of common functions provided in the NCAR command language (NCL). This might cause problems in areas of high orography and inside the planetary boundary layer. These areas are not considered in the following analysis. ~~Both are avoided in the following application.~~

3. ~~Consider to first separate the fluctuations from the background with appropiate numerical or dynamical filters.~~ The method can handle any kind of variables. For the present application, we choose the horizontal divergence. While this quantity was available in the retrievals, other data source might require its calculation from the wind fields. However, if other variables are preferred, here is the step to calculate them.

4. The underlying Hilbert transform ~~starts~~is implemented with a Discrete Fourier Transform (DFT) which creates a complex ~~series~~spectrum in wave number space $\hat{f}_k$ from the real valued data f_x in real space (e.g. Smith et al. (1997)). The processing of the three-dimensional data in the (x, y, z)-space is begun with the $x-$direction. The mathematics behind the Hilbert transform is described briefly for an one-dimensional function f_x originating in real space:

$$f_k = \mathrm{DFT}(f_x) \tag{1}$$

The index $_k$ denotes the wave number space, $_x$ describes the function f in real space.

5. DFTs can be biased by variance leakage through side lobes in spectral space. Tapering methods abandon this but can smear out nearby wave numbers. A loss of absolute amplitude can be overcome by using normalised weights (e.g. Von Storch and Zwiers, 2001). For the present study, however, the best results were obtained by turning the taper off.

6. In wave number space a rectangular bandpass filter reduces the complex ~~series~~spectrum to the user-predefined wave number limits k_{min} and k_{max}. Here, we make sure that only waves of the considered range of wave numbers are used for the following analysis.

$$f_{k,filtered} = F(k_{min}, k_{max}) f_k. \tag{2}$$

7. To get back from wave number space an inverse DFT is performed.

$$\hat{f}_x = 2 * \mathrm{DFT}^{-1}(f_{k,filtered}). \tag{3}$$

8. The such constructed complex-valued function $\hat{f}_x$ consists of the input data f_x as the real part and the Hilbert-transformed function $H(f_x)$ as the imaginary part

$$\hat{f}_x = f_x + iH(f_x). \tag{4}$$

It provides the amplitude a_x (Schönwiese, 2013)

$$a_x = |\hat{f}_x| = \sqrt{{f_x}^2 + H(f_x)^2} \tag{5}$$

and the phase estimate Φ_x

$$\Phi_x = \mathrm{atan}\left(\frac{H(f_x)}{f_x}\right). \tag{6}$$

9. The phase gradient is a measure of the wave number modulus

$$k_x = \frac{d\Phi_x}{dx} \approx \frac{\left|\mathrm{DFT}^{-1}(k\mathrm{DFT}\hat{f}_x)\right|}{|\hat{f}_x|}. \tag{7}$$

10. Due to the finite character of the data series it may happen that high-frequency spurious fluctuations appear after the Hilbert transform. We ~~neglect~~damp them ~~those~~ by applying a low-pass filter. We smooth over a number of grid points determined by the lower wave number limit k_{min}.

11. Alienation of outliers is taken care of by two different quality checks. Firstly, the amplitude and wave number are checked for at least a half undamped wave. Therefore, the packet length l_x is essential. It is calculated by covariance functions C_{xx}:

$$l_x = \sum_{x=0}^{x_{max}} \left|\frac{C_{xx}}{C_{00}}\right| \tag{8}$$

with $x_{max} = \frac{N-1}{5}$ (Chatfield, 2016). This method goes back to Zülicke and Peters (2006). The quality check then is defined by the inequality

$$k_x l_x > \pi. \tag{9}$$

Secondly, the retrieved signals are ~~supposed~~required to lie above the noise level of the input data. An empirical threshold c checks the amplitude for being valid considering the standard deviation of the input ~~horizontal divergence δ~~ function $\sigma(f_x)$

$$a_x > c * \delta(f_x)\sigma(f_x). \tag{10}$$

Empirically, we use $c = 0.01$. This idea follows Glatt and Wirth (2014).

UWaDi uses a quality flag $q = 1$ which is set to false ($q = 0$) if at least one quality check is rejected.

12. Steps 4 to 9 are repeated for the other dimensions (y, z).

13. Amplitude and absolute wave number are saved on the same grid as the input data to create a full three-dimensional analysis of local wave quantities. The amplitude is combined to a wave number-weighted sum of the three spatial dimensions

$$a_{(x,y,z)} = \left(\frac{\sum_{d=x,y,z} q_d k_d^2 a_d^2}{\sum_{d=x,y,z} q_d k_d^2}\right)^{\frac{1}{2}}. \tag{11}$$

The absolute wave number is determined by

$$k_{(x,y,z)} = \left(\sum_{d=x,y,z} q_d * k_d^2 \right)^{\frac{1}{2}}, \tag{12}$$

with d denoting the spatial index.

The method provides an exact measure of the amplitude in the sense of the sum of squared amplitudes of the wave modes. The dominating wave number is the amplitude weighted sum of all. Spectrally wide dynamics can cause a significant reduction of information (Appendix A). Applying UWaDi with several narrow band-pass limits would provide information on spectrally spread waves. The wave numbers are estimated as moduli, that is: the three-dimensional wave number $(\pm k_x, \pm k_y, \pm k_z)$ allows for eight possible directions. However, the method is recommended for the first guess of the dominant wave packet including the derivation of the intrinsic frequency from the dispersion relation.

2.2 Validation of the method

For a comparison of ~~available~~wave characteristics obtained with different methods ~~that obtain wave quantities~~ we choose the test case presented in Zimin et al. (2003) (Fig. 1a). In this excersice, a~~A~~ couple of localiz~~z~~ed wave packets with the wave numbers 4 and 9 is given in one dimension on the interval $[0, 4\pi]$ by

$$f_x = \exp\left(-(x-4.5)^2\right)\cos(4x) + \exp\left(-(x-7.5)^2\right)\cos(9x). \tag{13}$$

Here, the quality check (step 11) requires the amplitudes to exceed half of the sample standard deviation.
UWaDi based on a Hilbert transform is a continuous method working without any box parameter. 3D ST, S3D and DIV need box-width parameters to be adapted to the corresponding scientific case. A compromise between accuracy in space and wave number has to be found. For DIV the box length is set to $L^{DIV} = 8.0$ which covers the largest anticipated wavelength. For 1D ST, which was modified from 3D ST, two steering parameters have to be adapted to the present task. We find a box width factor of $C_L^{1DST} = 0.25$ suiting our requirements. Next to that, 1D ST provides a correction factor for the absolute amplitude value C_A^{1DST}. In three-dimensional data analyses enormous amplitude reduction can occur. Artificially changing the amplitude impacts the variance conservation of the technique. This is why we choose $C_A^{1DST} = 1$ for our example. For S1D a fixed box length has to be determined in advance. We find $L^{S1D} = 1.5$ to give acceptable results. We note that an extension to three dimensions would add information and therefore, accuracy. However, in order to realise comparability we stay with the strictly one-dimensional setup.

The method showing the best agreement with the theoretical value is UWaDi (Fig. 1b). For the amplitude both wave packets are clearly distinguishable and the maximum peaks are recovered exactly. ~~As expected, the 3D ST~~1D ST and S1D ~~method shows a~~ rebuild~~ing of~~ the wave packet~~'s~~ shape as well. The lack of absolute amplitude value might be ~~overcome~~adjusted with empirical correction factors provided for 1D ST. Nevertheless, the amplitudes of both wave packets differ from each other. ~~A higher peak of amplitude is given by the DIV method but the two wave packets are smeared out.~~ DIV provides a smeared

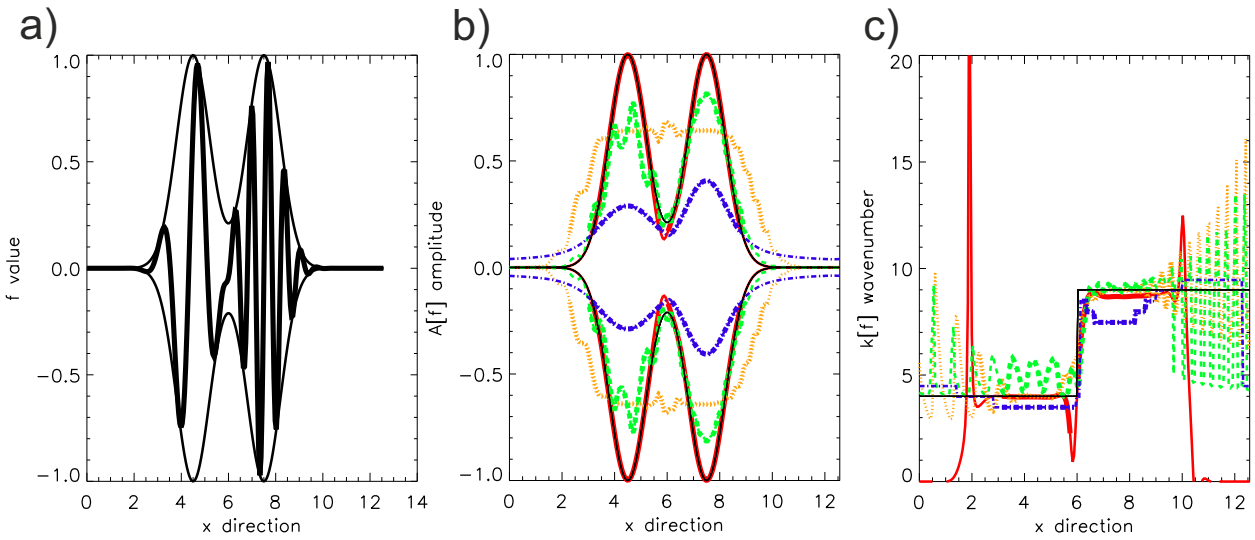

Figure 1. One-dimensional test function (a) bold line) adapted from Zimin et al. (2003) and its envelope (a) thin line). Comparison of amplitude (b) and wave number (c) calculated by different methods: UWaDi (solid, red), DIV (dotted, orange), S1D (dashed, green) and 1D ST (dash-dotted, blue). Valid estimates are drawn in bold.

out wave-packet envelope. ~~A similar pattern is shown for the S-3D method. Both latter methods show high dependence on the chosen box size withing the analysis.~~ The wave number calculation is best for UWaDi (Fig. 1c). The high peaks at the beginning and end of the wave packets are sorted out by the quality check. ~~S-3D and 3D-ST show good results in peaking at the right value but do not cover the complete spatial range of the wave packet. Wave number calculation of DIV shows higher deviations.~~ DIV meets the right wave numbers as well, but does not cover the whole spatial range of the two wave packets. 1D ST and S1D show small deviations from the expected values. Altogether, UWaDi shows ~~nearly perfect~~the best agreements with the theoretical expectations.

2.3 Analysis data

ECMWF data from the IFS operational cycle 41r1 is chosen for this analysis.~~Together with the latest cycle 41r2 it is based on T1279 L137 but differs in its effective horizontal resolution and non-orographic gravity wave parameterization. Cy41r2 reduces the distance between grid points to 9 km, from former 16 km.~~ ~~Not shown~~We performed comparison studies between IFS data ~~provided~~ on different grid sizes $(0.1°, 0.36°, 1°)$. By considering our bandpass filter conditions ~~gave~~we found reliable ~~and comparable~~ results for the $0.1°$- and $0.36°$-grids. ~~Therefore, we decide that the former cycle stored with~~To compromise between computational costs and stability of results we decide that data with a resolution of $0.36°$ (ca. 40 km) meet~~s~~ our requirements. They are retrieved from a resolution of T511. We discuss resolved gravity waves of a horizontal scale between 100 km and 1500 km. In vertical direction we are interested in gravity waves within the wavelength limits of 1 km to 15 km. These scales fu~~l~~lfill the assumption of hydrostatics and cover the range of mid- and low-frequency GWs (Guest et al., 2000).

Vertical propagating GWs are damped in ECMWF IFS products from 10 hPa (≈30 km) upwards (ECMWF, 2016). At 10 hPa the stratospheric sponge starts and a damping of wave propagation is expected (Jablonowski and Williamson, 2011). The mesospheric sponge follows at 1 hPa acting on the divergence and therefore directly on the GW properties. We restrict our analysis to a maximum altitude of 45 km and therefore follow the advice of Yamashita et al. (2010). The regular latitude-longitude grid is remained during the analysis.We interpolate model levels to equidistant height levels between 2 km to 45 km with a distance of 500 m and provide initial scientific analysis for a snapshot on 30 January 2016, 0 UTC corresponding to a minor SSW.

2.4 Gravity-wave specific quantities

From the diagnosed fields of amplitude and wave number we calculate the kinematic wave energy e and wave action A. In order to find the ageostrophic GW motion we analyse fields of horizontal divergence. The kinematic wave energy is derived from polarisation equations for GWs assuming hydrostatics (Zülicke and Peters, 2006) (Appendix B):

$$e = \frac{\delta^2}{k_h^2}. \tag{14}$$

In this formula we need information on the divergence variance and the horizontal wave number. Both are provided by UWaDi from the three-dimensional divergence field.

$$\delta^2 = \frac{a^2}{2} \tag{15}$$

$$k_h^2 = k_x^2 + k_y^2 \tag{16}$$

The wave action is a conserved quantity describing waves in presence of an inhogeneousinhomogeneous background wind field (Bretherton, 1966). It does not change for upward propagating waves as long as they do not interact with the mean flow.The wave action is a conserved quantity as long as the slowly varying wave packet does not interact with the mean flow, e.g. by dissipation, absorption or breaking (Bretherton, 1966). wWave action is defined by putting the kinematic wave energy e in relation to the intrinsic (flow-relative) frequency $\hat{\omega}$:

$$A = \rho \frac{e}{\hat{\omega}}, \tag{17}$$

ρ being the density. The intrinsic frequency $\hat{\omega}$ is calculated with the dispersion relation in mid- and low-frequency approximation: $\hat{\omega}^2 = f^2 + \frac{N^2\left(k_x^2+k_y^2\right)}{k_z^2}$.
From $A = \rho\frac{e}{\hat{\omega}}$ =constant, one can see the following

- density effect: $e \propto \frac{1}{\rho} \propto \exp\left(\frac{z}{H}\right)$. The above derived energy undergoes an exponential increase according to the density with the scale height H in vertical direction z.

– ~~wind effect: $e \propto \Omega$. From the apparent (ground-based) phase speed $c = \frac{\hat{\omega}}{k} + u$ one gets the dependence of the intrinsic frequency: $\omega = k(c - u)$. Assuming constant phase speed c and a constant wave number k for a wave packet, meaning that a wave is propagating in a horizontally homogenous wind $u(z)$, the energy scales with the background wind u.~~ wind effect: $e \propto u_h$. This relation holds for a stationary horizontally homogeneous mean flow $(u(z), v(z))$ which implies the invariance of the horizontal wave number (k_x =const and k_y =const) along with the apparent (ground-based) frequency ($\omega = \hat{\omega} + k_x u + k_y v = \hat{\omega} + k_h u_h \cos(\alpha_k - \alpha_u)$ =const). The energy scaling is obtained with the invariance of the wave action for an upwind wave ($\alpha_k \to \alpha_u + \pi$) as $e = \frac{A}{\rho}\hat{\omega} \to \frac{A}{\rho}\omega + k_h u_h$) due to the Doppler shift of the intrinsic (flow-relative) frequency (Marks and Eckermann, 1995).

For the following analysis primarily wave action is used.

3 Results

A minor SSW occurred on 30 January 2016. Fig. 2a shows the wind ~~velocity~~speed of the northern hemisphere at 10 hPa at 0 UTC. A vortex displacement from the pole is visible. The displaced vortex causes areas of strongly curved winds. ~~The jet streak above northern Europe is decelerating.The displaced vortex includes several jet streaks and areas of strongly curved winds.~~ The horizontal divergence as a measure of GWs shows high wave activity above two areas (Fig. 2b). Firstly, above northern Europe horizontal divergence is aligned cross-stream. Secondly, spiral-like~~Equal~~ patterns appear above eastern Siberia, corresponding to ~~another~~ an area of a ~~decelerating and bent wind~~curved jet streak. UWaDi applied on the field of horizontal divergence provides GW amplitude and wave action (Fig. 2c, d). ~~Areas of high orography like the Tibetan Plateau and Greenland are excluded.~~ GW amplitudes show patterns ~~aligned with the~~in regions of strongly alternating horizontal divergence. The wave action shows the highest peak above northern Europe and lower values above eastern Siberia. ~~In the zonal mean the horizontal wave number remains nearly constant with increasing altitude (Fig. 3). In more convenient terms of wavelengths, we find a horizontal variation between 130 km to 165 km. The vertical wave number decreases from the bottom limit to an altitude of 3 km. At the altitude of 10 km where the tropospheric jet is expected it shows a change in gradient. The increase in vertical wave number after 35 km altitude is a feature that occurs in the zonal mean data frequently, independent from the overall synoptic situation and is therefore expected to be an artefact of artifical wave damping from the IFS sponge layer. In wavelength, the vertical wave number in zonal mean varies between 2 km and 5 km.~~In zonal mean the horizontal wavelength varies between 120 km and 200 km (Fig 3a). In the mid-stratosphere between 18 km and 40 km altitude the horizontal wavelength remains nearly constant. Thus, our assumption of a homogeneous background wind field is approximately valid in the mid-stratosphere. The vertical wavelength scales from 2.2 km to 5.2 km. It increases throughout the whole atmospheric section with a slight change of gradient at the altitude of the tropopause (10 km). The decrease of vertical wavelength above 35 km altitude is dubious. It occurs frequently, also for other temporal snapshots. We suspect an influence of the IFS sponge layer but do not exclude an influence of the decreasing zonal wind, and therefore remain critical on interpretations in these altitudes. The horizontal phase speed in wave direction ($c_h = \frac{\omega}{k_h} = \frac{\hat{\omega}}{k_h} + u_h \cos(\alpha_k - \alpha_u)$) is approximated for an upwind wave ($c_h \to \hat{c_h} - u_h$). It remains unchanged for waves propagating passively through a stationary horizontally homogeneous wind field. The zonal

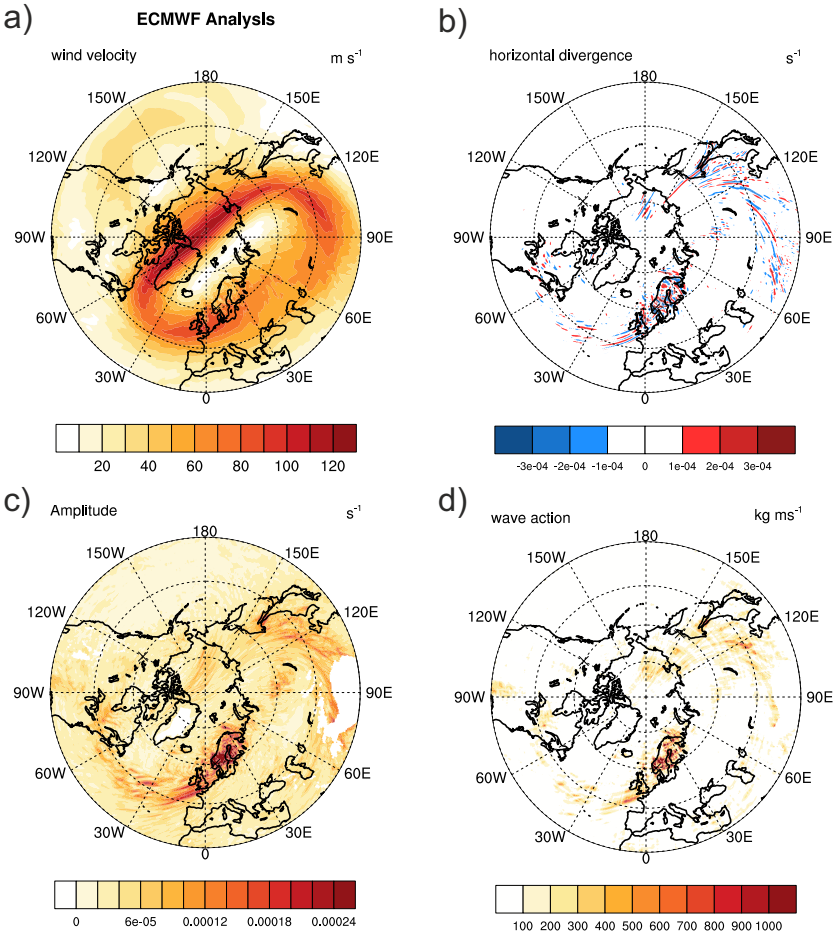

Figure 2. Synoptical situation of the northern hemisphere from ECMWF analysis at 10 hPa on 30 January, 2016. Wind speed (a), horizontal divergence (b). Gravity wave amplitude (c) and wave action (d). Circled numbers along the 60° N-latitude indicate positions of three vertical profiles for the later analysis.

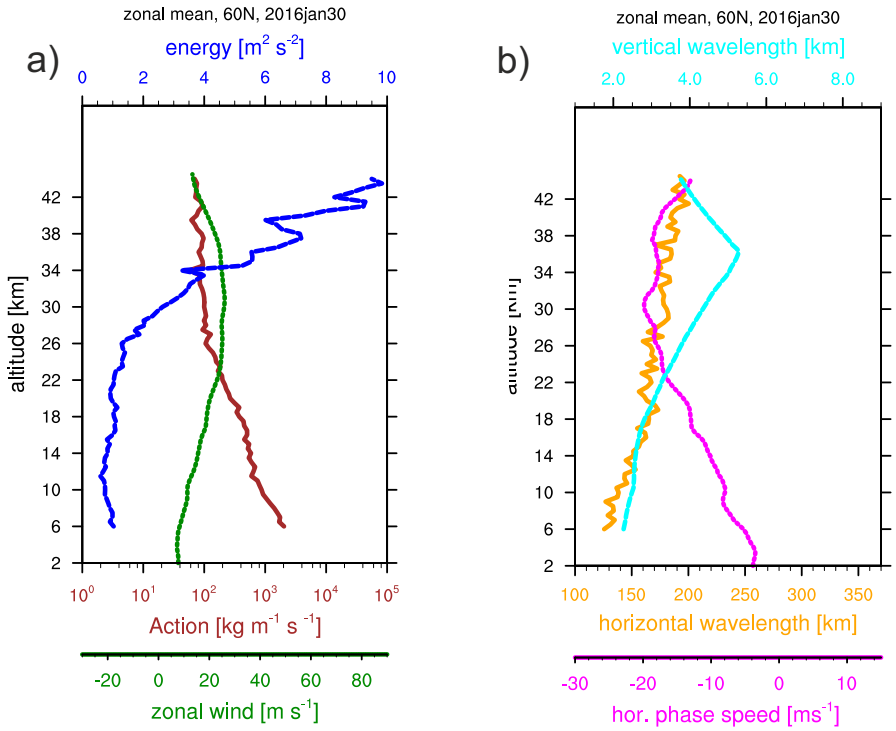

Figure 3. ~~Horizontal (solid, orange) and vertical (dotted, light blue) wavenumber~~Zonal mean profiles at 60 °N with a) zonal wind (green, dotted), energy (dark blue, dashed) and wave action (red, solid) and b) apparent horizontal phase speed (pink, dotted), vertical wavelength (light blue, dashed) and horizontal wavelength (orange, solid).

mean remains nearly constant with a value of 5 ms^{-1} below the tropopause and then steadily increases in the stratosphere (Fig. 3b). The indicated variations of horizontal wave number and phase speed contradict assumptions of a passive propagation through a stationary horizontally homogeneous wind field.

We next inspect local profiles in different background wind conditions. Longitude-height sections of zonal wind (Fig. 4a) and wave action (Fig. 4b) at 60° N ~~on 30 January 2016~~ help to find the location of interesting vertical profiles. Three profiles are chosen that are representative for regions of similar filter conditions. ~~We did not find significant differences between spatial averaging over areas of some longitudes extension and the local profiles (not shown). The low-pass filter applied in Step 10 helps to overcome massive grid-point to grid-point fluctuations.~~ The first profile ① at 7.56° E is chosen to be in a ~~height~~longitudinal range characterised by strong zonal eastward winds and lies in the deceleration area of the jet stream above northern Europe. Profile ② is at 151.92° E, therewith in the area of a ~~descented~~strongly curved stratospheric jet ~~streak caused by~~associated with the displacement of the polar vortex. In Fig. 4a it is visible as a wind intrusion in the altitude range between 14 km and 34 km. The wave action shows a peak in that height ~~area~~rage (Fig. 4b). For comparison we take a third profile ③ at 240.12° E in a region of low wind ~~velocity~~speed above Canada, that is: weak tropospheric and weak stratospheric jets.

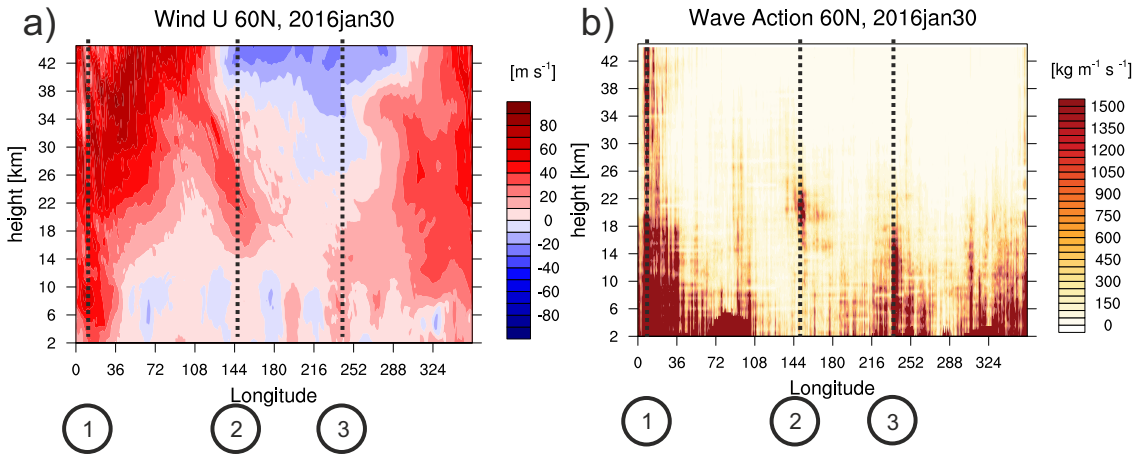

Figure 4. Zonal wind (a) and wave action (b) at 60°N, 30 January 2016 in longitude-height section. Numbered vertical profiles for further analysis are highlighted.

To highlight the advantage of a local wave analysis we ~~plot the zonal mean wave quantities at 60° N on 30 January 2016~~show profiles at selected longitudinal positions (Fig. 5a). ~~One can see the energy scaling with the decreasing density with increasing altitude. Small deviations from the exponential density structure correlate with small jumps in the wave action profile. Overall, zonal mean zonal wind is low with a small maximum hinting at the stratospheric jet stream. Wave action and kinematic wave energy are highly variable below 6 km altitude because of orographic influence. The not trustworthy areas are excluded. Overall, wave action decreases from 1000 $\mathrm{kg\,m^{-1}\,s^{-1}}$ in the upper troposphere to 100 $\mathrm{kg\,m^{-1}\,s^{-1}}$ in the middle atmosphere. Further upwards it remains constant. A constant profile of wave action means a constant propagation of GWs without deposition of momentum and therefore no interaction with the mean flow. The wind profile shows low wind speeds. We are interested in selective wave transmission which can not be seen from zonal mean averages. Thus, we provide local profiles.~~

During a local increase of wind ~~velocity~~speed above northern Europe the vertical profiles of ① show that the zonal wind meanders around 50 $\mathrm{m\,s^{-1}}$ (Fig. 5b). In the stratosphere, ~~T~~the vertical wavelength ~~number~~ is nearly constant with an average wavelength of 8 km which is higher in the troposphere with 11.5 km (not shown).~~and a small minimum after the tropospheric jet with 7 km. The low-pass filter acts on a spatial running average of $k_{min} = 15$km, therefore the wave number does not scale with the wind fluctuations~~ The wave action shows a high gradient changing from former ~~10000~~10^4 $\mathrm{kg\,m^{-1}\,s^{-1}}$ to ~~1000~~10^3 $\mathrm{kg\,m^{-1}\,s^{-1}}$~~, right where the vertical wave number has its maximum at an altitude of 16 km~~ and remains at this high level above 20 km.

Above eastern Siberia a ~~descended~~displaced stratospheric jet streak appears, jointly with high wave action (Fig. 4). The zonal wind vertical profile ② shows this in a height range of 14 km to 30 km with in increase from 5 $\mathrm{m\,s^{-1}}$ to maximal 30 $\mathrm{m\,s^{-1}}$ (Fig. 5c). The wave action follows the structure of the zonal wind. ~~The vertical wavenumber shows lower gradients in that altitude range. Altogether,~~Noteably, peak GW ~~emissions~~activity ~~seems to~~ take~~s~~ place in the lower stratosphere, clearly above

the tropospheric jet stream. At these altitude, GWs of vertical wavelength of 2 km ~~can be~~is found and the horizontal wavelength is about 350 km (Fig. 6).

The last set of vertical profiles is located in an area of low zonal winds ③ (Fig. 5d). In the troposphere eastward winds and in the middle stratosphere westward winds occur~~e~~ with magnitudes below 20 ms^{-1}. ~~In~~Above the altitude of the wind reversal ~~a change of gradient in~~the wave action ~~might show a filter process of GWs~~remains constant. ~~This profile lies in the lee of the Rocky Mountains, hence, mountain waves are most likely.~~

4 Discussion

The topic of selective wave transmission was first ~~risen up~~modeled by Dunkerton and Butchart (1984). They highlighted the longitude-dependent gravity wave propagation during an SSW by focussing on the impact on the mesosphere. Ern et al. (2016) further point out that the selective filtering by the anom~~o~~alous winds during an SSW create heavy impact on GW propagation through the whole atmosphere. They point out theoretically~~,~~ that during the upward~~s~~ propagation of GWs, these waves get attenuated or eliminated by distinct specifications of background flows. ~~These findings were obtained with the box-based S-3D algorithm. We add some spatially more refined analysis with UWaDi~~Here, we compare local vertical profiles of background wind and GW parameters from analysis data.

Comparing the three cases ①, ② and ③ with respect to their wave action profiles we diagnose at 42 km values ranging over three orders of magnitude. This confirms the high spatial variability of GWs during SSWs. Also the shapes of the profiles differ clearly. One class is characterised with a steady decrease up until 25 km and constance above (such as the zonal mean and cases ① and ③). Another class of profile shows a well-expressed peak in the stratosphere and a steady decrease above (case ②). The detailed analysis related GW dynamics goes beyond the scope of this paper. However, some hypotheses are formulated.

In the ~~The~~ high-wind case ①, showing the highest values of wave action and ~~nearly no changes~~weak in the vertical wave number above northern Europe, we find~~are defined by~~ the longest vertical wavelength ~~with 7~~of our study (8 km). ~~This long vertical wavelength describing~~These steep waves~~may~~ hint on an orographic~~excited~~ GW caused by the eastward flow above the ~~s~~Scandinavian mountain ridge Kjølen. ~~The location as well as the filtered out short vertical wavelengths suggest this idea and agree with findings of Limpasuvan et al. (2011). The overall high wave action underlines the orographic induced GW packet assumption. This is close to the findings of Krisch et al. (2017), who analysed a wave packet on 25 January 2016 above Iceland, just a few days before our analysis. Mentionable is that from the 25 January to 30 January the overall approaching flow direction did not change above northern Europe and comparable GW characteristics can be expected.~~This is comparable to findings of Limpasuvan et al. (2011) who showed that during the SSW 2009 westward propagating GW packets emanate from key topographical features around the polar edge and that these wave packets have long vertical wavelengths. Further detailed analysis on this GW packet are expected by upcoming publications according to the joint measurement campaign of ~~METROSI, GW-LCYCLE 2 and PACOG~~ROMIC and MS-GWaves at, amongst others, Kiruna, Sweden (67° N, 20° E).

In the ~~descended~~displaced stratospheric jet case ② (Fig. 5c) we find a GW packet triggered off a ~~bent~~curved ~~and decelerating~~ stratospheric jet streak. Firstly explained by Uccellini and Koch (1987), jet-exit regions in the troposphere are expected to emit

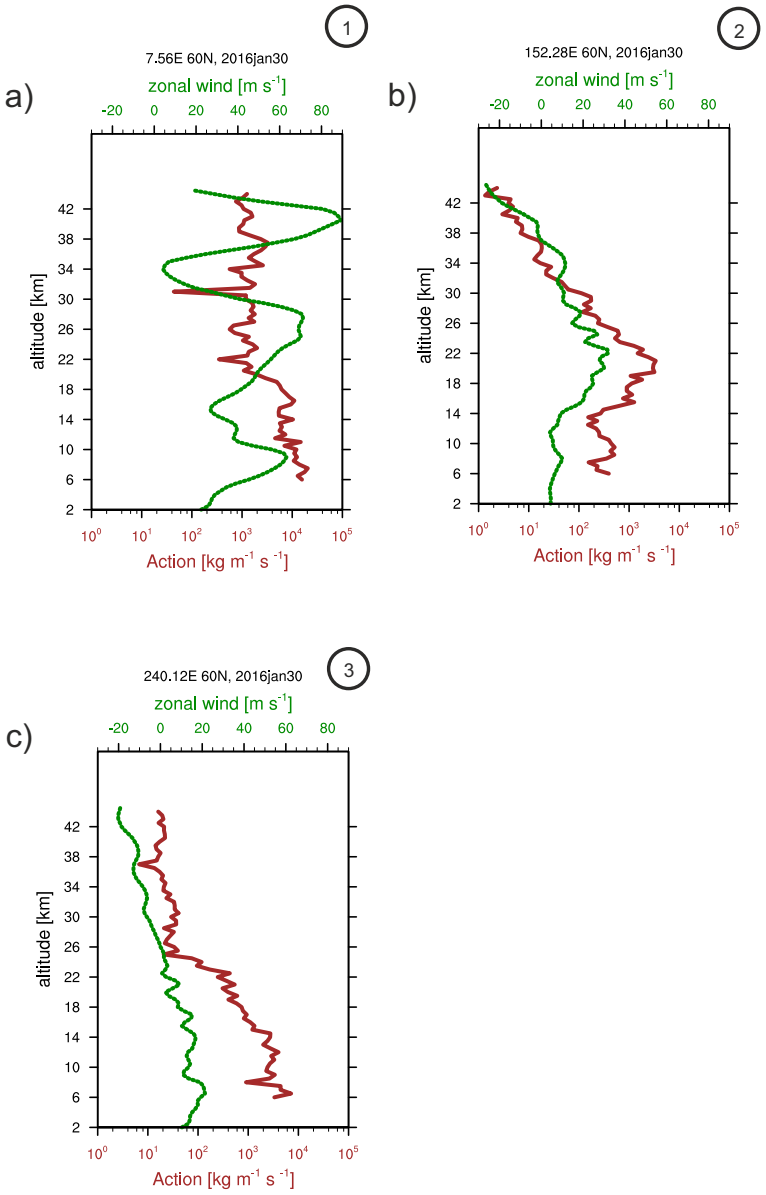

Figure 5. Vertical profiles at 60°N, 30 January 2016. ~~Zonal mean (a) of kinematic wave energy (dotted, blue), wave action (solid, red) and zonal wind (dashed, green).~~ Local vertical profiles at 7.56°E (~~b~~a), 151.92°E (~~c~~b) and 240.12°E (~~d~~c) with the ~~vertical wavenumber (dotted, light blue),~~ wave action (solid, red) and zonal wind (dashed, green). Local profiles according to markers ~~of~~in Fig. 4.

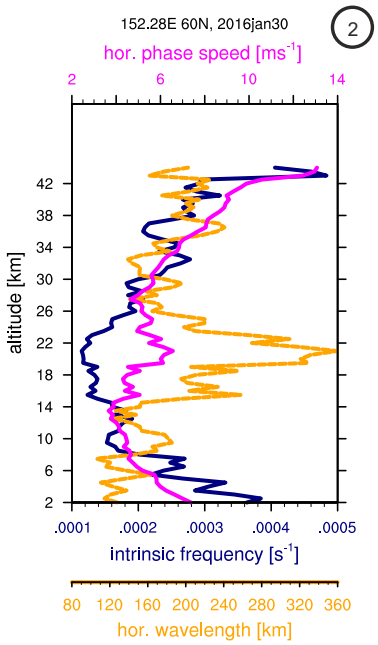

Figure 6. Intrinsic frequency (bold, dark blue), horizontal wavelength (dashed, orange) and horizontal phase speed (bold, pink) for profile ② (Fig. 5c).

GWs. The increase of wave action in the middle stratosphere according to the intrusion of westerlies seen in Fig. 4a and b leads to the assumption that the present feature is ~~caused by~~associated to the stratospheric jet. The horizontal divergence field supports this hypothe~~th~~sis with ~~cross-stream aligned fluctuations~~GW structures spiraling out of the curved jet above eastern Siberia~~,~~. These feautures are comparable to the ~~findings in~~simulations of the troposphere by Mirzaei et al. (2014) which resolved shallow near-inertia waves in jet-exit regions. Further ~~agreements~~hints are the higher wave action as well as the ~~lowest shown~~smallest found wavelength ~~in this case of~~ (1.9 km) along the largest found horizontal wavelength (350 km). ~~Wave packets found in jet-exit region are characterised as shallow near-inertial wave packets.~~

~~Furthermore, we want to discuss the phenomenon of vanishing GWs at critical wind levels. Stating that waves orthogonal to the mean flow are eliminated due to critical layer absorption occures if the wave vector rotates (Dunkerton and Butchard, 1984). With local vertical profiles of the vertical wavenumber we find these features above the descended stratospheric jet in ②. The critical level is the level at which background wind and GW phase speed are of same value. There, GWs dissipate and drag is put on the mean flow at lower altitudes than during undisturbed conditions (Wang and Alexander, 2009). Here, a peak in vertical wave number is an indicator for wave absorption according to the mid-frequencies dispersion relation and definition of the Doppler frequency: $k_z = \frac{N}{(c-u)}$. At winds of the order of the phase speed the denominator reduces to zero and the vertical wave number peaks. In an altitude of 28 km we see a peak in the vertical wave number where the zonal wind reaches $u \approx 15 \mathrm{m\,s^{-1}}$. We find a horizontal phase speed of $c \approx 15 \mathrm{m\,s^{-1}}$, which measures up with the expectations because~~

~~jet-generated GWs tend to be fast. The decrease of wave action quantifies the filtering of GWs in this height range. A sharp jump to less wave action is not expected as we apply the low-pass filter and it may take the length of one wave to be filtered out. Furthermore, due to the relative high phase speed no sharp variation at the height of the wind reversal is visible. The near-inertial GWs are not subject of absorption.~~

In the low-wind case ③ ~~we see that the vertical wavenumber does not directly scale with the low zonal wind. The~~the high wave action in the upper troposphere up to the height of the wind reversal of 23 km ~~may~~might be caused by orographic induced GWs due to the position in the lee of the Rocky Mountains. ~~Assuming to have orographic quasi-stationary GWs, we get a horizontal phase speed of $c \approx 0\,\mathrm{m\,s^{-1}}$ and do not find absorption at critical levels except at the height of the wind reversal, where a high gradient in wave action is visible.~~ Above that, the overall lowest values of wave action are found, aggreeing with measurements in that height range (Thurairajah et al., 2010). It is interesting to note, that the shape of the wave action profile is similar to the zonal-mean profile (compare Fig. 3a and Fig. 5c) while the wind above 25 km goes into another direction. ~~The feature of increasing vertical wave number above an altitude of 35 km fits to our findings before, where in zonal mean vertical wave number we saw the sponge layer of the model to begin to act on GWs (Fig. 3). We suggest, the fact that we do not see this in the other profiles arises from the low wind speeds jointly with low phase speed for this case. In zonal mean we do find low zonal winds as well (Fig. 5a).~~

5 Summary and Conclusion

With UWaDi we provide a tool for the analysis of ~~any wave-containing~~gridded three-dimensional data to estimate amplitude and wave number phase-independently and locally. The method is based on a Hilbert transform and returns~~such~~ an estimate for each data grid point, thus, avoiding the use of pre-defined boxes for ~~a spectral estimate~~the analysis. With regard to the locality it clearly shows its advantages in a method comparison for a~~n~~ synthetic test case. Disadvantages may play a role when the wave spectrum is broad and the ~~nomination~~attribution of the variance to one dominant harmonic is not justified. The additional estimation of the wave numbers completes the elements of a wave packet description. Their sign is not fixed which is the case for all spatial analysis methods considered in this paper. However, the method is recommended as a reliable local ~~estimate~~diagnosis of medium complexity.

For the analysis of gravity waves, we estimated wave energy and wave action from the horizontal divergence. This approach does not require an explicit numerical filtering which is a practical advantage. Other methods for the analysis of unbalanced flow components are available, although more complicated (Mirzaei et al., 2017). While the chosen formulae requires the variance (or squared amplitude) and wave numbers, ~~UWaDi~~the Hilbert transform method may also provide local estimates for more complex ~~tools~~procedures such as the combined Rossby wave and gravity wave diagnostics of Kinoshita and Sato (2013). ~~There, cross-covariances of different quantities are needed.~~ For our study, which is focused on hydrostatic inertia-GW~~s~~ appearance, the specific approach is optimal.

With the ~~short~~demonstrative analysis of the synoptic situation on 30 January 2016 we show the advantages of UWaDi: providing wave quantities on every grid point. Longitude-dependent GW filter processes, known as selective wave transmission, can be

~~analysed~~diagnosed spatially in detail. ~~We find that in zonal mean no prominent GW features can be seen during a mSSW vortex displacement. Instead,~~lLocal vertical profiles show selective wave transmissions ~~relative to the zonal mean profiles~~and generation processes. ~~During strong eastward winds GW propagation is high at all altitudes, the vertical wave number does not show strong variation, thus indicating a steadily vertical propagation of GWs. We find the source of the GWs in the troposphere and characterise this case as induced by flow over orography. Further, critical layer absorption is visible. The wave case with overall low zonal wind reveals gradients in wave action at the altitude of a wind reversal.~~We found cases with steady decrease of the wave action through the tropopause up to the mid-stratosphere and constant values above in contrast to a case with a strong peak in the lower stratosphere and a steady decrease above. The latter happened in~~Unexpectingly, we see the influence of the ECMWF sponge layer in the stratosphere which starts to flatten GWs at an altitude of 35 km in situations of weak winds and slow waves. In~~ an area where the wind field is effected by the mSSW, ~~we find~~characterised with a curved ~~and decelerating~~ jet stream-exit region in the stratosphere and ~~suggest that GWs are emitted there~~discuss GW generation by spontaneous emission. The diagnosed long horizontal and short vertical wavelengths support this hypothesis. With the present method we plan to join the closer evaluation of observations and models with respect to local features of GW generation and propagation.

Code and data availability. The data from ECMWF is accessible through the archive of www.ecmwf.int provided by the Deutscher Wetterdienst. The code named UWaDi is available through the authors. It is coded in open-source software and a user's manual can be provided. The authors request to cite this paper in case of applying the UWaDi algorithm.

Appendix A: Estimates for two-wave mixture

In this section we illustrate mathematically the amplitude and wave number estimates for a superposition of waves. For simplicity, imagine a mixture of two waves which have amplitudes changing on much larger scales than the lengths of the carrier waves

$$f = a_1 \cos(k_1 x + \phi_1) + a_2 \cos(k_2 x + \phi_2). \tag{A1}$$

The Hilbert transform creates

$$H = a_1 \sin(k_1 x + \phi_1) + a_2 \sin(k_2 x + \phi_2). \tag{A2}$$

The local amplitude is calculated by

$$a^2 = f^2 + H^2. \tag{A3}$$

~~and~~ It contains terms with equal wavelengths (the desired squared sines and cosines) as well as mixed-wavelength~~s~~ terms which are either slow ($\pm(k_1 - k_2)$) or fast ($\pm(k_1 + k_2)$). The application of the low-pass filter (Step 10) is intent~~d~~ed to eliminate the fast spurious components which are expected to create the most fuzziness. With this procedure ~~supposed to work~~we find from

the equal-wave number termns the sum of all squared amplitudes

$$a^2 = a_1^2 + a_2^2. \tag{A4}$$

This means: all variance is included in this estimate. For the wave numbers we find from the definition

$$k^2 = \frac{k_1^2 a_1^2 + k_2^2 a_2^2}{a_1^2 + a_2^2}. \tag{A5}$$

This is the amplitude-weighted sum of squared wave numbers.

The covariance (or squared standard deviation) is the mean of squares:

$$s^2 = \langle f^2 \rangle = \langle a_1^2 \cos^2(k_1 x + \phi_1) + a_2^2 \cos^2(k_2 x + \phi_2) \rangle = \frac{a_1^2}{2} + \frac{a_2^2}{2} = \frac{a^2}{2} \tag{A6}$$

Hence, the ensemble average results in half of the squared amplitude.

Appendix B: Derivation of ~~kinematic~~total wave energy

The total wave energy is composed of kinetic and potential energy ($e_{tot} = e_{kin} + e_{pot}$). The following considerations are related to linearised equations in Boussinesq approximation in a resting environment (e.g. Gill, 1982). We use the ~~polarisation equations for hydrostatic GWs to express the kinetic energy with~~definitions of horizontal divergence $\delta = -\mathrm{i}(k_x u + k_y v)$ and vorticity $\xi\zeta = -\mathrm{i}(k_x uv - k_y vu)$ to rewrite the kinetic energy as

$$e_{kin} = \frac{1}{2}(u^2 + v^2) = \frac{1}{2}\frac{\delta^2 + \xi\zeta^2}{k_h^2}. \tag{B1}$$

The potential energy is expressed with the buoyancy tendency $-\mathrm{i}\omega b = -N^2 w$ to yield

$$e_{pot} = \frac{1}{2}\frac{b^2}{N^2} = \frac{1}{2}\frac{N^2 w^2}{\omega^2}. \tag{B2}$$

~~i~~In order to express the total energy in terms of the divergence, both formulae are combined with the vorticity tendency $-\mathrm{i}\omega\xi\zeta = -f\delta$ and the continuity equation ($\delta = -\mathrm{i}k_z w$) ~~for~~

$$e_{tot} = \frac{1}{2}\left(\frac{\delta^2}{k_h^2}\left(1 \pm \frac{f^2}{\omega^2}\right) \pm \frac{N^2}{\omega^2}\frac{\delta^2}{k_z^2}\right). \tag{B3}$$

The final result is obtained with incorporation of the dispersion relation for hydrostatic inertia-GWs $\omega^2 = f^2 + N^2 \frac{k_h^2}{k_z^2}$ reading

$$e_{tot} = \frac{\delta^2}{k_h^2}. \tag{B4}$$

Competing interests. The authors declare that no competing interests are present.

Acknowledgements. We acknowledge the funding of the research unit Multiscale Dynamics of Gravity Waves / project Spontaneous Imbalance by the Deutsche Forschungsgemeinschaft (DFG) through grant ZU 120/2-1. Furthermore the authors want to thank the ECMWF for data supply. Useful comments on this manuscript were given by Vivien Matthias and Steffen Hien. Special thanks go to one of the reviewers for provision of program code and check values.

References

Albers, J. R. and Birner, T.: Vortex preconditioning due to planetary and gravity waves prior to sudden stratospheric warmings, Journal of the Atmospheric Sciences, 71, 4028–4054, 2014.

Alexander, M. J. and Vincent, R. A.: Gravity waves in the tropical lower stratosphere: A model study of seasonal and interannual variability, Journal of Geophysical Research: Atmospheres, 105, 17 983–17 993, 2000.

Andrews, D. G., Holton, J. R., and Leovy, C. B.: Middle atmosphere dynamics, 40, Academic press, 1987.

Bretherton, F. P.: The propagation of groups of internal gravity waves in a shear flow, Quarterly Journal of the Royal Meteorological Society, 92, 466–480, 1966.

Butler, A. H., Seidel, D. J., Hardiman, S. C., Butchart, N., Birner, T., and Match, A.: Defining sudden stratospheric warmings, Bulletin of the American Meteorological Society, 96, 1913–1928, 2015.

Chatfield, C.: The analysis of time series: an introduction, CRC press, 2016.

Coy, L., Newman, P. A., Pawson, S., and Lait, L. R.: Dynamics of the Disrupted 2015/16 Quasi-Biennial Oscillation, Journal of Climate, 30, 5661–5674, 2017.

Dörnbrack, A., Pitts, M. C., Poole, L. R., Orsolini, Y. J., Nishii, K., and Nakamura, H.: The 2009-2010 arctic stratospheric winter-general evolution, mountain waves and predictability of an operational weather forecast model, Atmospheric Chemistry and Physics, 12, 3659, 2012.

Dörnbrack, A., Gisinger, S., Pitts, M. C., Poole, L. R., and Maturilli, M.: Multilevel cloud structures over Svalbard, Monthly Weather Review, 145, 1149–1159, 2017.

Dunkerton, T. J.: The role of gravity waves in the quasi-biennial oscillation, Journal of Geophysical Research: Atmospheres, 102, 26 053–26 076, 1997.

Dunkerton, T. J. and Butchart, N.: Propagation and selective transmission of internal gravity waves in a sudden warming, Journal of the Atmospheric Sciences, 41, 1443–1460, 1984.

ECMWF: Part III: Dynamics and Numerical Procedures, IFS Documentation, ECMWF, 2016.

Ehard, B., Kaifler, B., Dörnbrack, A., Preusse, P., Eckermann, S. D., Bramberger, M., Gisinger, S., Kaifler, N., Liley, B., Wagner, J., et al.: Horizontal propagation of large-amplitude mountain waves into the polar night jet, Journal of Geophysical Research: Atmospheres, 122, 1423–1436, 2017.

Ern, M., Ploeger, F., Preusse, P., Gille, J., Gray, L., Kalisch, S., Mlynczak, M., Russell, J., and Riese, M.: Interaction of gravity waves with the QBO: A satellite perspective, Journal of Geophysical Research: Atmospheres, 119, 2329–2355, 2014.

Ern, M., Thai, Q., John, C., Martin, G., James, M., and Michael, J.: Satellite observations of middle atmosphere gravity wave absolute momentum flux and of its vertical gradient during recent stratospheric warmings, Atmos. Chem. Phys, 1680, 7324, 2016.

Ern, M., Hoffmann, L., and Preusse, P.: Directional gravity wave momentum fluxes in the stratosphere derived from high-resolution AIRS temperature data, Geophysical Research Letters, 44, 475–485, 2017.

Fritts, D. C. and Alexander, M. J.: Gravity wave dynamics and effects in the middle atmosphere, Reviews of Geophysics, 41, doi:10.1029/2001RG000106, 1003, 2003.

Garcia, R. R. and Solomon, S.: The effect of breaking gravity waves on the dynamics and chemical composition of the mesosphere and lower thermosphere, Journal of Geophysical Research: Atmospheres, 90, 3850–3868, 1985.

Gill, A. E.: Atmosphere-Ocean dynamics (International Geophysics Series), academic press, 1982.

Glatt, I. and Wirth, V.: Identifying Rossby wave trains and quantifying their properties, Quarterly Journal of the Royal Meteorological Society, 140, 384–396, 2014.

Guest, F. M., Reeder, M. J., Marks, C. J., and Karoly, D. J.: Inertia–gravity waves observed in the lower stratosphere over Macquarie Island, Journal of the Atmospheric Sciences, 57, 737–752, 2000.

Holton, J. R.: The Influence of Gravity Wave Breaking on the General Circulation of the Middle Atmosphere, Journal of the Atmospheric Sciences, 40, 2497–2507, 1983.

Jablonowski, C. and Williamson, D. L.: The pros and cons of diffusion, filters and fixers in atmospheric general circulation models, in: Numerical Techniques for Global Atmospheric Models, pp. 381–493, Springer, 2011.

Jewtoukoff, V., Hertzog, A., Plougonven, R., de la Cámara, A., and Lott, F.: Comparison of gravity waves in the Southern Hemisphere derived from balloon observations and the ECMWF analyses, Journal of the Atmospheric Sciences, 2015.

Kalisch, S., Preusse, P., Ern, M., Eckermann, S. D., and Riese, M.: Differences in gravity wave drag between realistic oblique and assumed vertical propagation, Journal of Geophysical Research: Atmospheres, 119, 10,081–10,099, doi:10.1002/2014JD021779, 2014.

Khaykin, S., Hauchecorne, A., Mzé, N., and Keckhut, P.: Seasonal variation of gravity wave activity at midlatitudes from 7 years of COSMIC GPS and Rayleigh lidar temperature observations, Geophysical Research Letters, 42, 1251–1258, 2015.

Kinoshita, T. and Sato, K.: A formulation of three-dimensional residual mean flow applicable both to inertia–gravity waves and to Rossby waves, Journal of the Atmospheric Sciences, 70, 1577–1602, 2013.

Kramer, R., Wüst, S., Schmidt, C., and Bittner, M.: Gravity wave characteristics in the middle atmosphere during the CESAR campaign at Palma de Mallorca in 2011/2012: Impact of extratropical cyclones and cold fronts, Journal of Atmospheric and Solar-Terrestrial Physics, 128, 8–23, 2015.

Krisch, I., Preusse, P., Ungermann, J., Dörnbrack, A., Eckermann, S. D., Ern, M., Friedl-Vallon, F., Kaufmann, M., Oelhaf, H., Rapp, M., Strube, C., and Riese, M.: First tomographic observations of gravity waves by the infrared limb imager GLORIA, Atmospheric Chemistry and Physics Discussions, 2017, 1–21, 2017.

Lehmann, C., Kim, Y.-H., Preusse, P., Chun, H.-Y., Ern, M., and Kim, S.-Y.: Consistency between Fourier transform and small-volume few-wave decomposition for spectral and spatial variability of gravity waves above a typhoon, Atmospheric Measurement Techniques, 5, 1637–1651, 2012.

Limpasuvan, V., Alexander, M. J., Orsolini, Y. J., Wu, D. L., Xue, M., Richter, J. H., and Yamashita, C.: Mesoscale simulations of gravity waves during the 2008–2009 major stratospheric sudden warming, Journal of Geophysical Research: Atmospheres, 116, 2011.

Liu, H.-L. and Roble, R. G.: A study of a self-generated stratospheric sudden warming and its mesospheric–lower thermospheric impacts using the coupled TIME-GCM/CCM3, Journal of Geophysical Research: Atmospheres, 107, ACL 15–1–ACL 15–18, doi:10.1029/2001JD001533, 4695, 2002.

Manney, G. L. and Lawrence, Z. D.: The major stratospheric final warming in 2016: dispersal of vortex air and termination of Arctic chemical ozone loss, Atmospheric Chemistry and Physics, 16, 15 371, 2016.

Marks, C. J. and Eckermann, S. D.: A three-dimensional nonhydrostatic ray-tracing model for gravity waves: Formulation and preliminary results for the middle atmosphere, Journal of the atmospheric sciences, 52, 1959–1984, 1995.

Matthias, V., Dörnbrack, A., and Stober, G.: The extraordinarily strong and cold polar vortex in the early northern winter 2015/2016, Geophysical Research Letters, 43, 2016.

Mirzaei, M., Zülicke, C., Mohebalhojeh, A. R., Ahmadi-Givi, F., and Plougonven, R.: Structure, energy, and parameterization of inertia–gravity waves in dry and moist simulations of a baroclinic wave life cycle, Journal of the Atmospheric Sciences, 71, 2390–2414, 2014.

Mirzaei, M., Mohebalhojeh, A. R., Zülicke, C., and Plougonven, R.: On the quantification of imbalance and inertia-gravity waves generated in numerical simulations of moist baroclinic waves using the WRF model, Journal of the Atmospheric Sciences, in press, doi:10.1175/JAS-D-16-0366.1, 2017.

Plougonven, R., Teitelbaum, H., and Zeitlin, V.: Inertia gravity wave generation by the tropospheric midlatitude jet as given by the Fronts and Atlantic Storm-Track Experiment radio soundings, Journal of Geophysical Research: Atmospheres, 108, doi:10.1029/2003JD003535, 4686, 2003.

Preusse, P., Ern, M., Bechtold, P., Eckermann, S., Kalisch, S., Trinh, Q., and Riese, M.: Characteristics of gravity waves resolved by ECMWF, Atmospheric Chemistry and Physics, 14, 10 483–10 508, 2014.

Sato, K., Kinoshita, T., and Okamoto, K.: A new method to estimate three-dimensional residual-mean circulation in the middle atmosphere and its application to gravity wave–resolving general circulation model data, Journal of the Atmospheric Sciences, 70, 3756–3779, 2013.

Schönwiese, C.-D.: Praktische Statistik für Meteorologen und Geowissenschaftler, Schweizerbart'sche Verlagsbuchhandlung, 2013.

Shutts, G. and Vosper, S.: Stratospheric gravity waves revealed in NWP model forecasts, Quarterly Journal of the Royal Meteorological Society, 137, 303–317, 2011.

Smith, S. W. et al.: The scientist and engineer's guide to digital signal processing, 1997.

Stober, G., Matthias, V., Jacobi, C., Wilhelm, S., Höffner, J., and Chau, J. L.: Exceptionally strong summer-like zonal wind reversal in the upper mesosphere during winter 2015/16, Annales Geophysicae, 35, 711–720, 2017.

Thurairajah, B., Collins, R. L., Harvey, V. L., Lieberman, R. S., Gerding, M., Mizutani, K., and Livingston, J. M.: Gravity wave activity in the Arctic stratosphere and mesosphere during the 2007–2008 and 2008–2009 stratospheric sudden warming events, Journal of Geophysical Research: Atmospheres, 115, 2010.

Uccellini, L. and Koch, S.: The synoptic setting and possible source mechanisms for mesoscale gravity wave events, Mon. Weather Rev, 115, 721–729, 1987.

Vincent, R. A. and Fritts, D. C.: A climatology of gravity wave motions in the mesopause region at Adelaide, Australia, Journal of the Atmospheric Sciences, 44, 748–760, 1987.

Von Storch, H. and Zwiers, F. W.: Statistical analysis in climate research, Cambridge university press, 2001.

Wright, C. J., Hindley, N. P., Hoffmann, L., Alexander, M. J., and Mitchell, N. J.: Exploring gravity wave characteristics in 3-D using a novel S-transform technique: AIRS/Aqua measurements over the Southern Andes and Drake Passage, Atmospheric Chemistry and Physics, 17, 8553, 2017.

Yamashita, C., Liu, H.-L., and Chu, X.: Gravity wave variations during the 2009 stratospheric sudden warming as revealed by ECMWF-T799 and observations, Geophysical Research Letters, 37, doi:10.1029/2010GL045437, l22806, 2010.

Yamashita, C., England, S. L., Immel, T. J., and Chang, L. C.: Gravity wave variations during elevated stratopause events using SABER observations, Journal of Geophysical Research: Atmospheres, 118, 5287–5303, 2013.

Zimin, A. V., Szunyogh, I., Patil, D., Hunt, B. R., and Ott, E.: Extracting envelopes of Rossby wave packets, Monthly Weather Review, 131, 1011–1017, 2003.

Zimin, A. V., Szunyogh, I., Hunt, B. R., and Ott, E.: Extracting envelopes of nonzonally propagating Rossby wave packets, Monthly Weather Review, 134, 1329–1333, 2006.

Zülicke, C. and Becker, E.: The structure of the mesosphere during sudden stratospheric warmings in a global circulation model, Journal of Geophysical Research: Atmospheres, 118, 2255–2271, 2013.

Zülicke, C. and Peters, D.: Simulation of inertia-gravity waves in a poleward-breaking Rossby wave, Journal of the Atmospheric Sciences, 63, 3253–3276, 2006.